Journal of proteome research

pubs.acs.org/jpr

Article

In Vitro Exposure of A549 and J774A.1 Cells to SiO_2 and TiO_2 Nanoforms and Related Cellular- and Molecular-Level Effects: Application of Proteomics

Published as part of the Journal of Proteome Research special issue "Canadian Proteomics".

Premkumari Kumarathasan,* Nazila Nazemof, Erica Blais, Krishna Priya Syama, Dalibor Breznan, Yasmine Dirieh, Hiroyuki Aoki, Sadhna Phanse, Azam Tayabali, and Mohan Babu

Cite This: *J. Proteome Res.* 2025, 24, 1672−1687

Read Online

ACCESS | Metrics & More | Article Recommendations | Supporting Information

ABSTRACT: There is an emerging interest in incorporating proteomic data for environmental health risk assessments. Meanwhile, the production and use of engineered nanomaterials (ENMs) with attractive physicochemical properties are expanding with the potential for exposure, thus necessitating toxicity information on these materials for health risk analysis, where proteomic data can be informative. Here, cells (A549 human lung epithelial and J774A.1 mouse monocyte/macrophage cells) were exposed to ENMs (nanoforms of $SiO_2$and TiO_2) of different sizes and surface chemistries (dose: 0−100 $\mu g/cm^2$, 24 h) for *in vitro* toxicity data. Cytotoxicity (CTB, ATP, and LDH), oxidative stress (GSH oxidation), and proteomic analysis (MS- and antibody-based) were conducted post-nanoparticle (NP) exposure to determine the relative potency and identify perturbed cellular pathways. Dose-, nanoform-, and cell type-specific cytotoxicity changes were observed upon exposure to both nanoSiO_2 and nanoTiO_2. Size, agglomeration, surface modification, and metal impurities appeared to be the determinants of cytotoxicity. Proteomic analysis identified some enriched mechanistic pathways and biological processes relevant to cell defense/phagocytosis, stress, metabolism, apoptosis, and inflammatory processes in J774A.1 cells exposed to these NPs. A549 cells exhibited enriched pathway/biological processes relevant to transport/endocytosis, stress, metabolism, and inflammatory processes post-NP exposures. Concordance was observed between the nanoform exposure- and cell type-related cytotoxicity responses, notably cellular ATP, which is critical for cell viability, oxidative stress, and cellular pathways/biological processes. These findings demonstrate the application of proteomics in regulatory toxicology and warrant further research in this direction.

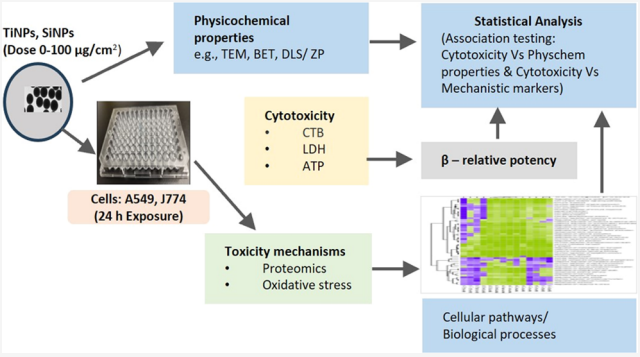

KEYWORDS: *nanoSiO_2, nanoTiO_2, in vitro toxicity, nanoforms, oxidative stress, proteomics, cellular pathways*

INTRODUCTION

Exposure to environmental chemicals ranging from toxic heavy metals to organic pollutants (e.g., plasticizers, per and polyfluoroalkyl substances, and flame retardants) and air pollutants (ambient air particulate matter including nanosized particles) are linked to various adverse health effects.[1−7] In recent years, engineered nanomaterials (ENMs) that are intentionally designed to have attractive unique physicochemical properties, including smaller sizes (<100 nm), high surface areas, surface modifications, and optical, catalytic, electrical, and magnetic properties have led to their use in various applications including electronics, cosmetics, food packaging/additives, and biomedicine.[8] Growing interest in ENM applications has led to increased production and use of these materials, enhancing the probability of exposure of humans and the ecosystem to these nanosized materials, thus causing human health concerns.[9,10]

The presence of nanoscale forms of existing substances in commerce has been identified in Canada and is on the Domestic Substances List (DSL) that requires toxicity information for assessment of associated health risks. Among these materials are the inorganic oxide-based ENMs, amorphous nanoSiO_2, and nanoTiO_2.[11]

Silica nanoparticles (SiNPs), including mesoporous and amorphous forms, have found widespread use in bioimaging,

Received: July 29, 2024
Revised: November 22, 2024
Accepted: January 29, 2025
Published: March 4, 2025

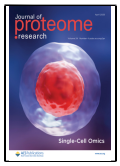

https://doi.org/10.1021/acs.jproteome.4c00651
J. Proteome Res. 2025, 24, 1672−1687

drug delivery, sensors, semiconductors, cosmetics, food additives, pesticides, and other consumer products.[10,12−17] Some desired physicochemical properties of SiNPs include large surface area, biocompatibility, potential degradability, adjustability, and mechanical strength.[18] Based on annual production, SiNPs are ranked second highest in the global market and are among the top 5 widely used ENMs in consumer products.[9,10] Meanwhile, nanoTiO_2 particles (TiNPs) are also largely produced ENMs with about 4 million tons in global production and are used in biomedical, electrical, and consumer applications such as photocatalysts, textiles, UV-resistant paints, cosmetics, toothpaste, sunscreens, food additives, and water treatment agents.[19−24] Since TiO_2 bulk material is known to be relatively less toxic,[25] it provides an impetus for nanoTiO_2 to be considered in various applications. However, emerging evidence suggests that the nanosize of a chemical compound can be relatively more potent than the bulk material, leading to concern regarding exposure to nanoTiO_2[26,27] and similar to nanoSiO_2.

There are several emerging reports on *in vitro* and *in vivo* toxicity testing of nanoSiO_2 and nanoTiO_2. Currently, chemical toxicity testing approaches are moving away from *in vivo* exposure models in support of efforts to reduce the use of vertebrate animals for chemical toxicity testing.[28,29] *In vitro* models are evolving as promising alternatives for toxicity screening studies supported by their low costs and high throughput, and enabled by emerging applications of high content of OMIC analyses to yield mechanistic information. Among the toxicity studies reported on nanoSiO_2, there are relatively more reports on mesoporous forms compared to amorphous nanoSiO_2.[30] Also, in general, the focus of many previous studies was to gain information on size-related toxicological effects of nanomaterials, including nanoSiO_2 and nanoTiO_2; thus, toxicity data are lacking for different nanoforms of the same chemical that have various applications.[31−36] Also, most of the *in vitro* exposure studies on nanoSiO_2 or nanoTiO_2 have reported on cytotoxicity or genotoxicity findings, and there are relatively few reports delving into toxicity mechanisms, with emerging studies on the use of transcriptomic analysis for this purpose.[37−40] In addition to the physicochemical properties of these nanomaterials, the high-content OMIC data that provide comprehensive molecular-level information (a new approach methodology, NAM) is of growing interest since it can add value to ENM exposure-related health risk analysis by advancing chemical grouping and read-across processes and by providing information on toxicity mechanisms.[41] Moreover, as mentioned above, a recent data gap analysis identified amorphous nanoSiO_2 and nanoTiO_2 among a number of engineered nanomaterials commercially available in Canada,[11] which required toxicity information for health risk assessment.

The objective of this study was to obtain information on the relative *in vitro* cytotoxic potencies of well-characterized amorphous nanoSiO_2 and nanoTiO_2 (pristine and surface-modified) nanoforms using multiple cell types relevant to the pulmonary toxicity of these nanoparticles (A549 human lung epithelial cells and J774A.1 mouse monocyte/macrophage cells), and the underlying toxicity mechanisms through high-content proteomic analysis. To achieve this, multiple cytotoxicity assays were conducted post-NP exposure to assess cell health, and physicochemical determinants of cytotoxicity were identified by testing for correlations between cytotoxic potencies of NPs and physicochemical properties. The mechanistic basis of toxicity was explored by testing for cellular oxidative stress and analyzing proteomic changes to gain information on cellular pathways/processes affected by exposure to these nanoforms. Reference bulk forms (microscale particles) were also included for cytotoxicity testing. In addition, concordance between cellular cytotoxicity, oxidative stress, and protein markers of inflammatory processes was tested to verify the potential links between key cellular events and cytotoxicity.

MATERIALS AND METHODS

Nanomaterials

NanoSiO_2 (SiNPs). Custom-synthesized amorphous silicon dioxide nanoparticles (SiNPs), uncoated pristine (15, 30, 50, 75, 100 nm) and surface-modified (−C_3-COOH, −C_{11}-COOH, −NH_2, and −PEG), were obtained from Advanced Quantum Materials Inc. (AQM, Edmonton, AB, Canada).

NanoTiO_2 (TiNPs). Ti-01 aeroxide, NIST SRM, anatase 19 nm, and rutile, 37 nm (uncoated); Ti-02 Kronos, surface-treated Al, Si, and Zr (coated); Ti-03 anatase, 50 nm mkNano (uncoated); Ti-04 anatase, 100 nm mkNano (uncoated); Ti-05 rutile, 50 nm mkNano (uncoated); Ti-06 anatase, < 5 nm, mkNano (uncoated); Ti-07 anatase/rutile, 20 nm, silica-coated; Ti-08 anatase/rutile, 20 nm, silica + alumina-coated; Ti-09 anatase/rutile, 20 nm silica + stearic acid-coated; Ti-10 anatase/rutile, 20 nm, silica + silicone oil-coated; and Ti-11 Sigma nanowire ($0.1 \times 100\ \mu m^2$) were obtained from Dr. L. Johnston of the National Research Council of Canada (Ottawa, ON, Canada). The reference particles included in this work were amorphous nanoSiO_2 (12 nm, Sigma-Aldrich, ON, Canada) and bulk TiO_2 (SRM154b, NIST, Gaithersburg, MD) for the *in vitro* cytotoxicity analysis.

Physicochemical Characteristics

The chemical composition of particles was tested by inductively coupled plasma mass spectrometry and atomic emission spectrometry (ICP-MS/-AES, Varian Vista-Pro, Mulgrave, Australia) on acid-digested (50% HNO_3, 8 h at 80 °C) filtered samples following previously reported methodologies[42] (duplicate analyses). The following analyses were performed at the NRC Laboratory (Dr. L. Johnston, NRC, Canada) using previously reported methods:[43,44] transmission electron microscopy (TEM) was performed using the dispersed particles on Formvar TEM grid (carbon film-covered copper grids), and samples were imaged using an FEI Technai G2 Spirit Twin TEM operated at 120 kV to measure size and shape of the particles; Brunauer−Emmett−Teller (BET) specific surface areas were measured by nitrogen adsorption using the ASAP 2020 System from Micromeritics (GA); the hydrodynamic diameter was measured (triplicate analyses) in liquid media (e.g., DMEM with FBS, water, or ethanol) by dynamic light scattering (DLS), and the surface charge was measured by ζ-potential (ZP) measurements using a Zetasizer Nano ZS (Malvern Instruments, UK); and thermogravimetric analysis (TGA) was performed to assess the surface group coverage using TA Instruments Q500 IR (Waters Limited, ON, Canada).

Endotoxin Analysis

The particle preparations mentioned above were analyzed for bacterial endotoxins using the chromogenic Limulus Amebocyte Lysate (LAL; Lonza, MD) test, as reported previously.[35]

Preparation of Nanoparticle Solutions for Dosing Cells

All stock solutions of ENMs (SiNPs and TiNPs) were prepared ($3\ mg\ mL^{-1}$) in deionized water, vortexed for 30 s, and sonicated in a bath sonicator (100 W, 20 kHz, VWR Ultrasonic Cleaner)

https://doi.org/10.1021/acs.jproteome.4c00651
J. Proteome Res. 2025, 24, 1672−1687

for 20 min. (Note: All particle solutions used in this study were prepared fresh prior to each exposure.)

Exposure of Cells to Nanoparticles

Human alveolar type II epithelial (A549) cells and mouse ascites monocyte/macrophage (J774A.1) cells (ATCC, Manassas, VA) were maintained in Dulbecco's modified Eagle's medium (DMEM/high glucose) containing phenol red with 10% (v/v) fetal bovine serum (FBS) in a T-75 flask (Corning, NY) and incubated at 37 °C with 5.0% CO_2.[35] At 80% confluency, cells were detached and seeded in a 96-well plate at a density of 10,000 cells/well for A549 and 20,000 cells/well for J774A.1 in 100 μL of DMEM (phenol red-free (Hyclone)), with 10% FBS (Hyclone) and incubated for 24 h prior to particle exposure. Stock solutions of particles were diluted with DMEM (phenol red and serum-free) in water, sonicated for an additional 2 min, briefly vortexed, and 100 μL of the diluted particle solutions were added to cell monolayers that already contained 100 μL of DMEM containing 10% FBS to establish particle exposure doses (0−100 μg cm^{-2}). The final FBS concentration in the cell culture medium was 5%. After exposure to the particles, the cells were incubated at 37 °C with 5% CO_2 and 95% relative humidity for 24 h prior to any analysis. All exposure experiments were performed in triplicate with two technical replicates per exposure experiment, and particle exposures were performed under cell-free conditions in parallel to assess any interference with the cytotoxicity assays due to the presence of nanoparticles. Furthermore, the cells, as well as supernatants, were clarified by centrifugation to ensure the removal of any traces of NPs prior to all analyses. Also, cell supernatants and cells treated with 100 μL of PBS containing Halt Protease Inhibitor cocktail (100×) (Thermo Scientific, Nepean, ON, Canada) were stored at −80 °C until further processing for proteomic analyses.

Cytotoxicity Analysis

Cellular cytotoxicity assays included analyzing the cellular ATP levels for cell metabolism, lactate dehydrogenase (LDH) released for cell membrane integrity, and Cell Titer-Blue (CTB) reduction for cell viability.

Cellular ATP levels were measured using the CellTiter-Glo luminescence assay kit from Promega. After 24 h of exposure to particles, the culture media was removed from the wells, replaced with 100 μL of fresh medium (5% FBS), equilibrated at room temperature (RT) for 30 min, and treated with 100 μL of CellTiter-Glo Reagent. The plate was shaken for 3 min on an orbital shaker to induce cell lysis and incubated at RT for 10 min to stabilize the luminescence signal. The supernatant was transferred to a 96-well V-bottom plate, centrifuged for 10 min at 2000 rpm, and the luminescence signal was read using a POLARstar Omega spectrophotometer plate reader (BMG Lab Tech, Ortenberg, Germany).

To determine the % LDH released, 150 μL aliquots of supernatants from particle-exposed J774A.1 or A549 cells were collected after 24 h, transferred to a 96-well V-shape plate, and centrifuged at 2000 rpm for 10 min. 50 μL of this clarified supernatant was treated with 50 μL of CytoTox-ONE assay reagent (Promega, Madison, WI). The stop solution from this assay kit was added to the reaction mixture after 10 min, and the absorbance was read at 490 nm using a POLARstar Omega spectrophotometer plate reader (BMG Lab Tech, Ortenberg, Germany). Similarly, control cells not treated with particles were lysed 24 h postexposure and analyzed for total LDH content, and these measurements were used to calculate the % LDH released.

Cell viability was assessed based on the premise that metabolically active viable cells can reduce the nonfluorescent dye Resazurin to fluorescent resorufin.[45] CellTiter-Blue Cell Viability Assay from Promega was used for this purpose. After 24 h of exposure, cell supernatants were removed and replaced with 100 μL of the fresh medium containing 20% CTB reagent (V/V) and incubated for 3 h at 37 °C. Fluorescence measurements were performed (λ_{Ex} = 573 and λ_{Em} = 600 nm) using a POLARstar Omega spectrophotometer (BMG Lab Tech, Ortenberg, Germany).

Statistical Analysis

Cytotoxicity data for the particle-exposed groups were normalized to the corresponding dose of zero controls to obtain the fold effect (FE) for each particle dose. A 3-way ANOVA analysis was conducted on SiNP data sets (for both cell types) with size, dose, and mod (modification) as factors. Meanwhile, for TiNPs, a 2-way ANOVA analysis was conducted with treatment and dose as factors on the FE data for cytotoxicity endpoints. Data were transformed (rank-transformed) to meet the conditions of normality and equal variance, as required. Multiple comparison testing was done using Holm−Sidak analysis. Also, potency estimate (β) was derived using FE = (dose + 1)$^{\beta}$, where β is the rate of change of dose with respect to the logarithm of the fold effect for a given endpoint[46] and was calculated using CurveExpert v1.4 (D. Hyams, TN). Pearson product-moment correlation analysis was performed to test for the associations between the physicochemical properties of NPs and NP cytotoxic potency β_{avg} values. Additional correlation tests were conducted using either Pearson product-moment correlation or Spearman correlation analysis to determine associations between cytotoxic potency β_{avg} values and cellular GSH/GSSG ratio (oxidative stress: Decrease in GSH/GSSG ratio), as well as cytotoxic potency β_{avg} values and inflammatory cytokines (IL-8 for A549 cells and TNFα for J774A.1 cells). All statistical tests were performed using SigmaPlot version 13.0 (Systat Software, San Jose, CA).

Mechanistic Analysis

Oxidative Stress. For cellular oxidative stress analysis, glutathione (GSH) and oxidized glutathione levels were measured using the GSH/GSSG-Glo assay following the manufacturer's instructions (Promega, Madison, WI). Briefly, cell supernatants were removed 24 h post-NP exposure (at 30 μg/cm^2), and 50 μL of the glutathione lysis reagent or oxidized glutathione lysis reagent was added to each well and the plate was shaken at RT for 5 min on a plate shaker. Then, 50 μL of the luciferin generation reagent was added to each well and the plate was shaken gently and incubated at RT for another 30 min, and 100 μL of the luciferin detection reagent was added to each well and shaken briefly. After 15 min, the luminescence signal was measured by using a POLARstar Omega Spectrophotometer Plate Reader (BMG Lab Tech, Ortenberg, Germany).

Proteomics Analysis

The secreted proteins in the cell culture supernatants were analyzed 24 h post-NP exposure (at a dose of 30 μg/cm^2) by the affinity-based targeted multiplex protein array methodology using a Milliplex MAP human multiplex panel or a mouse multiplex panel. The analysis was performed using the Bio-Plex Pro multiplex system (Bio-Rad, Hercules, CA) following previously reported procedures.[35,47]

Proteins in cell lysates were processed as follows: the frozen cells containing antiproteases were subjected to three freeze/

https://doi.org/10.1021/acs.jproteome.4c00651
J. Proteome Res. 2025, 24, 1672−1687

Table 1. Physicochemical Properties of SiNPs[a]

SiNP ID	TEM size (nm) (SD)	BET SA (m^2/g)	DLS size (nm)	PDI	ZP (mV)	total metals (ppm)	transition metals (ppm)	TGA functional groups (μmol g^{-1})
15 nm-P	17 (4)	29.6	657	0.54	−15.9	848	785	
30 nm-P	29 (4)	97.2	1128	0.72	−13.4	616	541	
75 nm-P	78 (6)	17	260	0.29	−16.6	476	419	
15 nm-C_3- COOH		162	531	0.50	−17.8			351
15 nm-C_{11}- COOH		20.1	445	0.44	−21.4			325
15 nm-NH_2		9.2	822	0.72	−6.7			1232
15 nm-PEG	14 (1)	19.6	528	0.47	−2.1			180

[a]TEM − transmission electron microscopy, SA − surface area, DLS − dynamic light scattering, PDI − polydispersity index, and ZP − ζ-potential.

Table 2. Physicochemical Properties of TiNPs[a]

TiNP ID	TEM size (nm)[b]	TEM size (nm)[c] (SD)	BET SA (m^2/g)	DLS size (nm)[d]	PDI	ZP (mV)	total Metals (ppm)	transition metals (ppm)	transition metal content (without Ti) (ppm)
Ti-01	28	19 (6)	54.2	154	0.14	40	517,160	517,070	41
Ti-02	350	209 (60)	16.5	296	0.16	42	506,268	486,657	37
Ti-03	50	30 (7)	82.4	200	0.37	−25	461,848	459,441	81
Ti-04	100	31 (10)	90.9	311	0.35	35	602,288	600,074	58
Ti-05	50	26 (8)	24.0	180	0.13	−29	513,808	510,838	161
Ti-06	5		152	31.7	0.15	33	455,888	455,742	90
Ti-07	20	38 (14)	45.5	484	0.36	−27	472,177	469,416	64
Ti-08	20	40 (13)	27.8	402	0.30	−26	479,422	458,413	100
Ti-09	20	36 (11)	40.8	256	0.18	−12	496,283	493,429	63
Ti-10	20	42 (15)	16.3	614	0.22	−40	452,244	446,071	53
Ti-11	100	790 (377)	23.6	513	0.33		478,281	399,787	54
TiO_2				513					

[a]TEM − transmission electron microscopy, SA − surface area, DLS − dynamic light scattering, PDI −polydispersity index, and ZP − ζ-potential. [b]Manufacturer's data. [c]NRC data. [d]Water except for Ti-09 and Ti-10 in ethanol, for DMEM with FBS medium values, see ref[69]. Ti-01 − anatase and rutile (uncoated); Ti-02 − surface-treated Al, Si, and Zr; Ti-03 − anatase (uncoated); Ti-04 − anatase (uncoated); Ti-05 − rutile (uncoated); Ti-06 − anatase (uncoated); Ti-07 − anatase/rutile, silica-coated; Ti-08 − anatase/rutile, silica + alumina-coated; Ti-09 − anatase/rutile, silica + stearic acid-coated; Ti-10 − anatase/rutile, silica + silicone oil-coated; Ti-11−nanowire (0.1 × 100 μm).

thaw cycles and were then treated with 1% sodium deoxycholate, vortexed, and sonicated for 10 min (with ice added to the bath), and were centrifuged at 10,000*g* for 10 min. The supernatants were fractionated using molecular weight cutoff filters (MWCO) to obtain fractions of 10−100 kDa, as described previously.[39] The filtrates obtained from MWCO fractionation were evaporated to complete dryness under a gentle stream of high-purity N_2 (g). These evaporated fractions were resuspended in 25 μL of 50 mM NH_4OAc (adjusted to pH 8), treated with 2 μL of ProteaseMax and 10 μL of Promega Trypsin Gold (Promega, Madison, WI), vortexed gently, centrifuged at 5000*g* (1 min), and incubated overnight in a water bath at 37 °C. These samples were treated with Trypsin-Lys C enzyme solution (50 μg/mL) for additional enzymatic digestion, vortexed gently, centrifuged at 5000*g* (1 min), and incubated for 4h in the water bath at 37 °C. The enzymatic digestion reaction was quenched with 5 μL of 5% TFA in deionized water, vortexed (3 s), and centrifuged at 14,000*g* (10 min) to remove any residues. Supernatants were stored at −80 °C for mass spectrometry analysis by LC-Orbitrap MS.

LC-MS/MS Analysis

Enzymatically digested peptide samples were desalted using ZipTip C_{18} pipette tips (Millipore Sigma, catalog number ZTC18S096, Darmstadt, Germany), according to the manufacturer's protocol, dried by evaporation using a Speed Vac concentrator (Savant), and stored at −20 °C prior to MS analysis. Before the MS analysis, the dried peptides were immediately resuspended in 0.1% FA. All samples were analyzed using nano-LC coupled to an Orbitrap Exploris mass spectrometer (Thermo Fisher Scientific). Chromatographic separation of the peptides was performed on a Proxeon EASY nLC 1200 System (Thermo Fisher Scientific) equipped with a Thermo Scientific Acclaim PepMap C18 column (15 cm × 50 μm ID, 3 μm, 100 Å), employing a water/ACN/0.1% FA gradient. 5 μL aliquots of reconstituted peptide samples were loaded on an LC column, and the flow rate was set at 0.6 μL/min. Peptides were initially separated with 1% ACN, which was increased to 3% ACN over 2 min, and then increased to 24% ACN over 45 min, followed by a linear increase to 80% ACN over 17 min and a wash period of 10 min with 80% of ACN. The eluted peptides were directly sprayed into a mass spectrometer using positive nanoelectrospray ionization (NSI) at an ion source temperature of 250 °C and an ion spray voltage of 2.1 kV. Full-scan MS spectra (375−1500 m/z) were acquired using Orbitrap Exploris at 120,000 (m/z 400) resolution. The automatic gain control settings were 1×10^6 for the full FTMS scans and 5×10^4 for the MS/MS scans. Fragmentation was performed by nanoelectrospray ionization (NSI) in a linear ion trap when the ion intensity was >1500 counts. The most intense ions were isolated for the ion trap NSI with charge states ≥2 and sequentially isolated for fragmentation using the normalized collision energy set at 35%, activation Q at 0.250, and an activation time of 10 ms. The ions selected for MS/MS analysis were dynamically excluded for 30 s. Calibration was performed externally using the Pierce FlexMix Calibration Solution (Thermo Fisher Scientific, catalog number 39239). The Orbitrap Exploris mass spectrometer was operated with

https://doi.org/10.1021/acs.jproteome.4c00651
J. Proteome Res. 2025, 24, 1672−1687

Table 3. Cytotoxic Potency of SiNPs in A549 and J774A.1 Cells

	A549 cells				J774A.1 cells			
	β				β			
NP	LDH	ATP	CTB	β_{avg}	LDH	ATP	CTB	β_{avg}
SiNP-12	0.065	0.037	0.01	0.037	0.355	0.36	0.263	0.326
SiNP-15P	0.04	0.033	0.015	0.029	0.068	0.027	0.006	0.034
SiNP-15 C3	0.01	0.018	0.018	0.015	0.001	0.012	0.005	0.006
SiNP-15 C11	0.053	0.008	0.008	0.023	0.011	0.024	0.009	0.015
SiNP-15 NH2	0.071	0.012	0.013	0.032	0.016	0.011	0.016	0.014
SiNP-15 PEG	0.002	0.021	0.01	0.011	0.001	0.026	0.001	0.009
SiNP-30 P	0.018	0.018	0.018	0.018	0.05	0.012	0.001	0.021
SiNP-30 C3	0.019	0.009	0.022	0.017	0.005	0.004	0.007	0.005
SiNP-30 C11	0.142	0.016	0.019	0.059	0.027	0.015	0.003	0.015
SiNP-30 NH2	0.083	0.051	0.046	0.06	0.06	0.008	0.012	0.027
SiNP-30 PEG	0.001	0.014	0.011	0.009	0.004	0.0001	0.007	0.004
SiNP-50 P	0.021	0.01	0.013	0.015	0.055	0.002	0.002	0.019
SiNP-50 C3	0.057	0.016	0.005	0.026	0.021	0.019	0.01	0.016
SiNP-50 C11	0.108	0.01	0.006	0.041	0.029	0.004	0.003	0.012
SiNP-50 NH2	0.021	0.024	0.004	0.016	0.027	0.001	0.008	0.012
SiNP-50 PEG	0.007	0.004	0.004	0.005	0	0.018	0.011	0.01
SiNP-75 P	0.019	0.009	0.002	0.01	0.114	0.021	0.022	0.052
SiNP-75 C3	0.009	0.001	0.006	0.005	0.01	0.006	0.012	0.009
SiNP-75 C11	0.02	0.007	0.001	0.01	0.016	0.007	0.018	0.014
SiNP-75 NH2	0.032	0.006	0.005	0.014	0.096	0.02	0.027	0.047
SiNP-75 PEG	0.006	0.006	0.005	0.006	0.002	0.002	0.019	0.008
SiNP-100 P	0.032	0.015	0.001	0.016	0.138	0.019	0.029	0.062
SiNP-100 C3	0.007	0.006	0.009	0.007	0.003	0.009	0.013	0.008
SiNP-100 C11	0.014	0.001	0.008	0.008	0.011	0.005	0.005	0.007
SiNP-100 NH2	0.016	0.005	0.03	0.017	0.026	0.001	0.013	0.013
SiNP-100 PEG	0.0004	0.048	0.007	0.018	0.013	0.015	0.001	0.01

Thermo XCalibur software. All RAW files were converted to mzXML using ReAdW-4.3.1.

Database searches of the A549 and J774A.1 SiNP and TiNP mzXML files were primarily carried out using MaxQuant version 1.6.7.0[48] against human (downloaded July 24, 2020) and mouse (downloaded July 24, 2020) protein sequence databases downloaded from UniProt.[49] To boost peptide and protein identifications, we also performed searches using two other search algorithms Tide from ms.Crux software suite version 1.0[50] and MSGF+ ver. 2020.08.05.[51] Search parameters were set to allow for two missed cleavages, trypsin digestion, and carbamidomethylation of cysteine as a fixed modification, while variable modifications were oxidation of methionine and acetylation of protein N-termini. The peptide search tolerance was set to 4.5 ppm for MS1, and the MS2 fragment tolerance was set to 20 ppm. Both false discovery rates at the peptide-spectrum match and protein levels were set to 0.1, and peptides with a minimum of 7 amino acids were considered for identification. A subsequent 1% false discovery rate by Percolator ver. 3.6[52] was applied for peptide identification. Mass spectrometry-based proteomics data were deposited to the MassIVE repository under the accession code "MSV000095579".

All protein fold-change data (normalized to controls) were used to conduct a preranked Gene set enrichment analysis (GSEA) pathway enrichment analysis[53] to determine pathways that were significantly up- or downregulated in each sample. The normalized enrichment scores (NES) were then hierarchically clustered using Cluster 3.0[54] and subsequently visualized as a heatmap in Java TreeView.[55] Furthermore, the fold-change cutoff was set at 1.5, $p < 0.05$, and a z score of 2 was used for the identification of canonical pathways and biological functions. Moreover, Gene ontology (GO) analysis was performed to identify biological processes.

RESULTS

Tables 1 and 2 illustrate the physicochemical properties of the nanoforms of SiO_2 and TiO_2 used in this work. TEM sizes in the dry state, BET surface area, DLS size for agglomeration in solution, ζ-potential for surface charge, and the extent of surface coating/functionalization results are from the TGA data. (Note: TEM images of these materials have been reported previously.[42,56]) The tables also provide information on the total and transition metal contents of these samples, as determined from the elemental analysis results. Among the pristine SiNPs, the 15 nm size form had the highest total and transition metal contents compared to the 30 and 75 nm SiNPs (Table 1). The BET surface area was higher for the 15 nm SiNP with surface modification $-C_3COOH$, as well as the 30 nm pristine SiNP form, while the DLS size was higher for the 15 nm SiNP with surface modification $-NH_2$, and the 30 nm pristine SiNP form compared to the rest of the SiNP forms. SiNPs with $-C_3COOH$ and $-C_{11}COOH$ surface groups displayed higher ZP (ζ-potential) values compared to the other SiNPs. Among the nanoforms of TiNPs, Ti-02 (surface-modified), Ti-04 (pristine), and Ti-11 (nanowire) displayed higher TEM sizes, while the DLS size was the highest for Ti-10 TiNP (Table 2).

The BET surface area values were higher for Ti-03 and Ti-04 TiNPs, while the ZP values were higher for Ti-01, Ti-02 (+ve), and Ti-10 (−ve) compared to other TiNPs. The total metal content was the highest for Ti-04, while the transition metal content (not including Ti content) was the highest for the Ti-05 TiNP form.

https://doi.org/10.1021/acs.jproteome.4c00651
J. Proteome Res. 2025, 24, 1672−1687

Table 4. Cytotoxic Potency of TiNPs in A549 and J774A.1 Cells

	A549 cells				J774A.1 Cells			
	β				β			
NP	LDH	ATP	CTB	β_{avg}	LDH	ATP	CTB	β_{avg}
Ti-01	0.0413	0.0172	0.0348	0.0311	0.0319	0.0095	0.0117	0.0177
Ti-02	0.0194	0.0075	0.0298	0.0189	0.0051	0.0052	0.0156	0.0086
Ti-03	0.0212	0.0206	0.0327	0.0248	0.0143	0.0131	0.0157	0.0144
Ti-04	0.0294	0.0094	0.0337	0.0242	0.0422	0.0200	0.0107	0.0243
Ti-05	0.0342	0.0051	0.0318	0.0237	0.0074	0.0205	0.0104	0.0128
Ti-06	0.0379	0.0045	0.0228	0.0217	0.0210	0.0163	0.0066	0.0147
Ti-07	0.0331	0.0017	0.0260	0.0203	0.0190	0.0133	0.0135	0.0153
Ti-08	0.0348	0.0057	0.0250	0.0218	0.0424	0.0192	0.0337	0.0318
Ti-09	0.0349	0.0141	0.0114	0.0201	0.0041	0.0177	0.0166	0.0128
Ti-10	0.0396	0.0269	0.0295	0.0320	0.0022	0.0140	0.0183	0.0115
Ti-11	0.0569	0.0348	0.0235	0.0384	0.0546	0.0196	0.0101	0.0281
TiO_2	0.0380	0.0268	0.0285	0.0311	0.0079	0.0218	0.0033	0.0110

Table 5. Relative Cytotoxic Potencies of SiNPs in A549 and J774A.1[a]

particle	SiNP-12	SiNP-15P	SiNP-15 C3	SiNP-15 C11	SiNP-15 NH_2	SiNP-15 PEG	SiNP-30 P	SiNP-75 P
				A549				
β_{avg}	0.037	0.029	0.015	0.023	0.032	0.011	0.018	0.01
rank	1	3	6	4	2	7	5	8
				J774A.1				
β_{avg}	0.326	0.034	0.006	0.015	0.014	0.009	0.021	0.052
rank	1	3	8	5	6	7	4	2

[a] $\beta_{avg.} = \beta(LDH) + \beta(ATP) + \beta(CTB)/3$.

Table 6. Relative Cytotoxic Potencies of TiNPs in A549 and J774A.1[a]

particle	Ti-01	Ti-02	Ti-03	Ti-04	Ti-05	Ti-06	Ti-07	Ti-08	Ti-09	Ti-10	Ti-11	TiO_2
						A549						
β_{avg}	0.031	0.019	0.025	0.024	0.024	0.022	0.02	0.022	0.02	0.032	0.038	0.031
rank	3	8	4	5	5	6	7	6	7	2	1	3
						J774A.1						
β_{avg}	0.018	0.009	0.014	0.024	0.013	0.015	0.015	0.032	0.013	0.012	0.028	0.011
rank	4	10	6	3	7	5	5	1	7	8	2	9

[a] $\beta_{avg} = \beta(LDH) + \beta(ATP) + \beta(CTB)/3$.

Table 7. Correlations between Cytotoxic Potencies (β_{avg}) of SiNPs and Physicochemical Properties

	β_{avg} for A549 cells vs					β_{avg} for J774A.1 cells vs			
Pearson correlation	TEM size (nm)	DLS size (nm)	SA[a] (m^2/g)	agglomeration SA[a]	TGA[b] (μmol/g)	DLS size[a] (nm)	DLS size[b] (nm)	ζ-potential[a] (mV)	TGA[b] (μmol/g)
R	−0.436	0.438	0.92	0.913	0.505	−0.928	0.661	−0.953	0.479
p	0.03	0.029	0.03	0.03	0.023	0.023	0.002	0.012	0.033

[a] Correlations were conducted only for pristine SiNPs. [b] Surface-modified SiNPs.

The relative *in vitro* potency values (β) for the different SiNP nanoforms assessed in this work for the two cell types based on individual cytotoxicity assays and also the corresponding consensus potencies (β_{avg}) are provided in Table 3. Excluding the positive control SiNP 12 nm, the uncoated pristine SiNP particles generally exhibited higher β values for % LDH release and ATP levels for both cell types (Table 3). Also, the SiNP nanoform exposure-related dose−response profiles for the different cytotoxicity endpoints and for the two cell types are depicted in Figures S1a−c and S2a−c. Here, 3-way ANOVA results revealed size- or dose-main effects or size X mod or dose X mod or size X dose interactions for both cell types, based on the assay. Meanwhile, for the TiNP nanoforms, with A549 cells, Ti-11 exhibited the highest β values for ATP and LDH assays compared to the other nanoforms, and with J774A.1 cells, Ti-08, Ti-11, and Ti-04 exhibited relatively higher β values for ATP and LDH assays (Table 4). The corresponding dose−response profiles for the different TiNP nanoform exposures in the two different cell types are shown in Figures S3a−c and S4a−c. The 2-way ANOVA results showed Treatment- and Dose-main effects for both cell types. In this work, endotoxin levels were negligible in these NPs (data not shown).

The average cytotoxic potency-based rankings are provided in Tables 5 and 6 for the SiNP and TiNP nanoforms for both A549 and J774A.1 cell exposure. Among the SiNPs, the smaller-sized pristine (uncoated) and coated ones were relatively more potent in A549 cells than in the J774A.1 cells, where the pristine SiNPs, both small and large particles, were relatively more potent.

https://doi.org/10.1021/acs.jproteome.4c00651
J. Proteome Res. 2025, 24, 1672−1687

Table 8. Correlations between Cytotoxic Potencies (β_{avg}) of TiNPs and Physicochemical Properties

	β_{avg} for A549 cells vs					β_{avg} for J774A.1 cells vs			
Pearson correlation	DLS[a]	DLS[b]	total metal content[b]	total metal content[c]	transition metal[c] (no Ti)	DLS[a]	TEM size[a]	transition metal[b] (no Ti)	BET SA[d]
R	0.766	0.826	−0.843	0.884	0.989	0.870	0.808	0.969	0.997
p	0.075	0.084	0.072	0.046	0.010	0.024	0.052	0.006	0.053

[a]Uncoated. [b]Coated. [c]Anatase/rutile (coated and uncoated). [d]Anatase (uncoated).

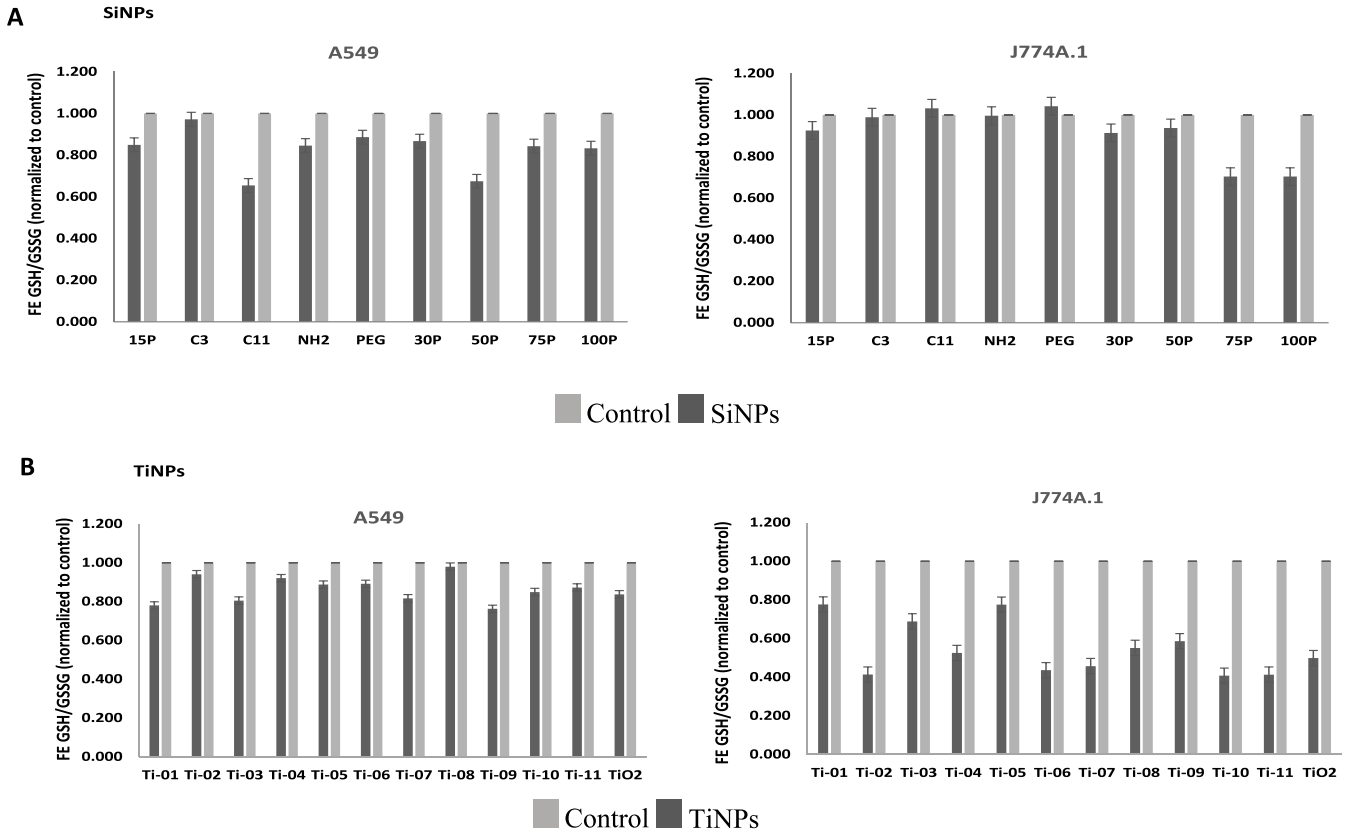

Figure 1. Oxidative stress levels (GSH/GSSG). Cellular oxidative stress measurements are expressed as mean fold change (FE) ± SE ($n = 3$) for A549 and J774A.1 cells exposed to different nanoforms (represented by the black bar) of (A) SiNPs (top panel) and (B) TiNPs (bottom panel), respectively. Cells without any treatment served as the control (represented by the gray bar). Oxidative stress levels in cells are measured by the ratio of GSH (glutathione reduced) to GSSG (glutathione oxidized).

However, with TiNPs, both uncoated Ti-01 and coated Ti-10, and nanowire Ti-11 were relatively more potent compared to other nanoforms in A549 while in J774A.1 cells, uncoated Ti-04, coated Ti-08, and nanowire Ti-11 were more potent than the other nanoforms.

Associations between the physicochemical properties of the SiNP and TiNP nanoforms and consensus average cytotoxic potency estimates "β_{avg}" are provided in Tables 7 and 8. SiNP toxic potencies were correlated with TEM, DLS sizes, SA and surface groups for A549 cell exposure, while SiNP potencies were correlated with DLS size, ZP, and surface groups for J774A.1 cell exposure. Meanwhile, for TiNPs, cytotoxic potency was correlated with the metal content in A549 cells, but in the J774A.1 cells, cytotoxic potency was related to the DLS size and metal content. There were borderline associations and trends observed between the NP potency and physicochemical properties (Tables 7 and 8).

Cellular oxidative stress levels followed by conversion of GSH (reduced form) to GSSG (oxidized form) after exposure of both cell types to the different nanoforms of SiNPs and TiNPs are illustrated in Figure 1A,B. All SiNP nanoforms displayed varying levels of cellular oxidative stress based on the cell type (Figure 1A), with relatively larger uncoated 75 and 100 nm SiNPs exhibiting increased oxidative stress in J774A.1 cells exposed to these particles. TiNP exposure resulted in increased cellular oxidative stress, with contrasting oxidative stress responses after exposure to different nanoforms based on the cell type (Figure 1B).

Gene set enrichment analysis (GSEA) results for enriched cellular pathways and biological processes after exposure of A549 and J774A.1 cells to the different SiNP and TiNP nanoforms are displayed in Figure 2. Green indicates down-regulation, and purple indicates upregulation. Dose- and nanoform-specific NP exposure responses were observed across different cell types. In general, the enriched pathways were related to cell signaling associated with various key cellular processes, including particle uptake, inflammatory processes, oxidative stress, cell cycle, metabolism, and cell death, namely apoptosis, as shown in Figure 3.

https://doi.org/10.1021/acs.jproteome.4c00651
J. Proteome Res. 2025, 24, 1672−1687

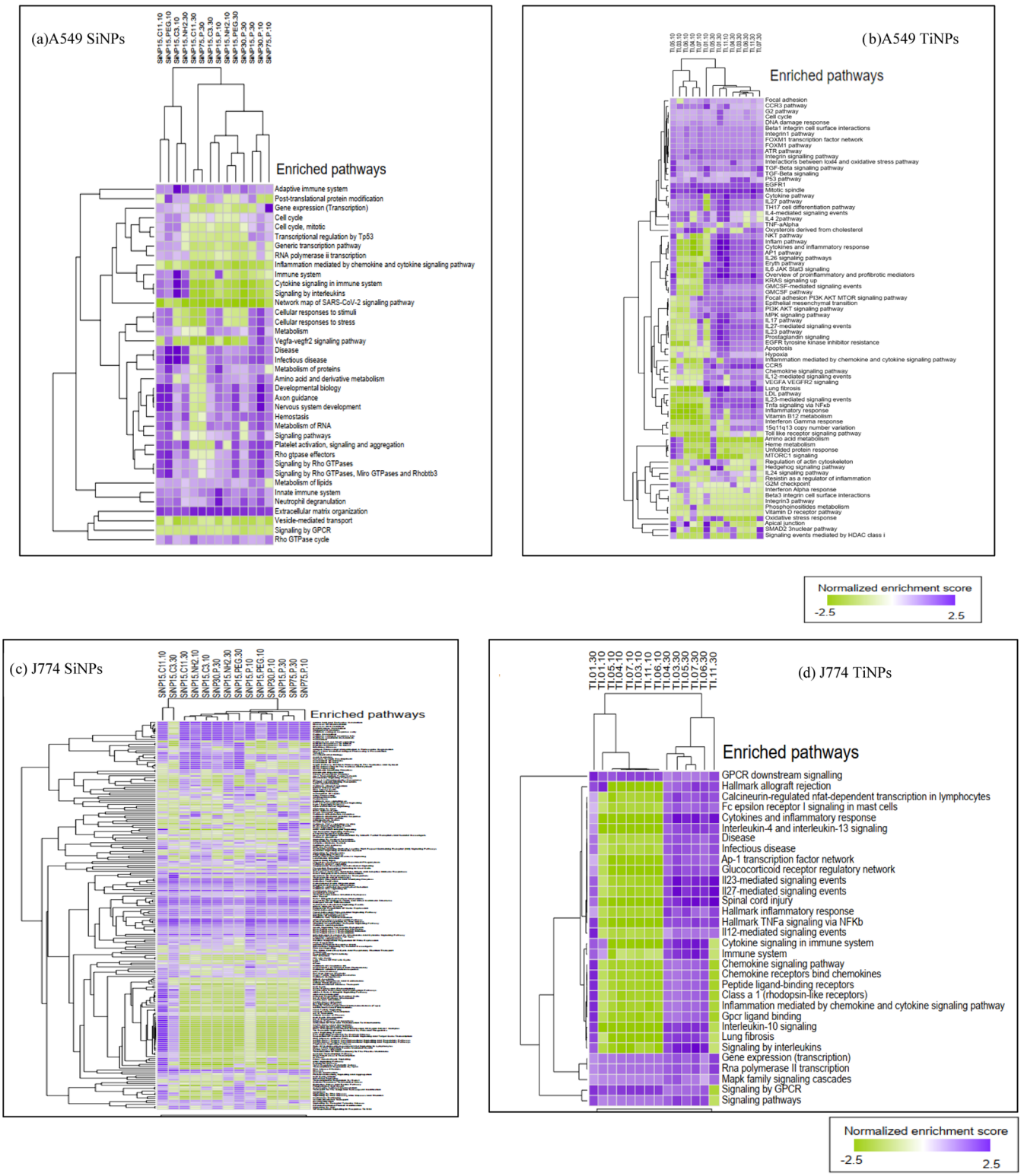

Figure 2. Heat map and hierarchical clustering of enriched cellular pathways (purple − upregulation; green − downregulation) for A549 and J774A.1 cells exposed to (a, c) SiNPs and (b, d) TiNPs from GSEA analysis of proteomic data.

DISCUSSION

Although there is extensive evidence supporting the utility of engineered nanomaterials such as nanoSiO_2 (SiNPs) and nanoTiO_2 (TiNPs) in various applications, including the biomedical field,[57,58] clarity is required in terms of the impact of these NP exposures on human health. Among the reports on toxicity testing of these nanomaterials, most studies have focused on size-related effects. Also, in general, toxicity studies on nanomaterials can suffer from the lack of adequate physicochemical characterization of nanomaterials, experimental artifacts arising from assay interferences caused by inherent optical properties of nanomaterials, and contaminants present in the nanoparticles based on routes of synthesis, which can lead to

https://doi.org/10.1021/acs.jproteome.4c00651
J. Proteome Res. 2025, 24, 1672−1687

Figure 3. Heat map and hierarchical clustering of biological processes affected (purple − upregulation; green − downregulation) in A549 and J774A.1 cells exposed to (a, c) SiNPs and (b, d) TiNPs.

inconsistencies in study findings, making comparisons of findings from different studies difficult. It has been noted that ENM should be considered on a case-by-case basis due to the heterogeneity in their physicochemical properties, which can influence their biological activity.[59−61] For instance, TiO_2 nanoparticles in some studies are reported to be less cytotoxic,[62] while others have reported exposure to these particles by the skin or pulmonary route and showed that these nanoparticles can induce oxidative stress, inflammation,[63] or genotoxicity.[64] Systematic studies with well-characterized nanomaterials and

https://doi.org/10.1021/acs.jproteome.4c00651
J. Proteome Res. 2025, 24, 1672−1687

defined protocols are needed to obtain a better understanding of the contribution of the physicochemical properties of these nanoparticles, including size, surface groups, solubility characteristics, and contaminants, on their relative toxicities[65−67] to enable comparison of toxicity findings. In addition, there is limited information on the toxicity of nanoforms of the same chemical, related mechanistic pathways, and physicochemical descriptors of potency required to support the assessment of associated health risks upon exposure to these materials.

Although the routes of exposure to nanoparticles can be inhalation, ingestion and/or dermal, in this work, we examined the *in vitro* toxicities of well-characterized nanoforms of amorphous SiO_2 (SiNPs) and TiO_2 (TiNPs) in multiple cell types relevant to the pulmonary toxicity of these particles to understand the effects related to the inhalation toxicity of these materials. Alveolar macrophages and epithelial cells are the gatekeepers of the lung as they are the first line of host defense and have an essential role in maintaining lung homeostasis.[68] In this context, we chose to use A549 human lung epithelial and J774A.1 mouse monocyte/macrophage cells. Species differences can also allow subsequent corresponding *in vitro−in vivo* validation studies as well as provide a comprehensive understanding of these nanoform toxicities. The influence of physicochemical factors on toxic potencies was also assessed in this study, and molecular-level information relevant to cytotoxicity was obtained by the analysis of oxidative stress as well as by application of high-content proteomic analysis. It should be noted here that the solubilities of nanoTiO_2 particles are low (<1%), as reported earlier,[69] and amorphous nanoSiO_2 particles are reported to be relatively slightly soluble (100 mg/L)[70] in contrast to other highly soluble inorganic oxide nanoparticles such as nanoZnO. Measures were taken in the conduct of exposure experiments in this work to avoid pitfalls in toxicity testing of NMs such as ensuring minimization/tracking of experimental artifacts due to optical interference in cytotoxicity assays by nanoparticles, analyzing the chemical composition of these nanoforms to assess contaminant-related toxicity, and supporting reliable health risk analysis.

Cytotoxicity data on the nanoforms of SiNPs identified size-, dose-specific, size x mod, dose x mod, and size x dose interactions, which were assay-specific and evident in both cell types (Figures S1a−c and S2a−c). Furthermore, cell type-specific changes in cytotoxicity endpoints were clear from the dose−response profiles. For instance, %LDH release, reflecting cell membrane integrity, was adversely affected by smaller-sized (e.g., 15 and 30, nm) particles (uncoated and coated) for A549 cells, while J774A.1 cells were affected by larger particles (e.g., 75 and 100 nm), as shown by the relative potency (β_{avg}) values (Tables 3 and 4). In addition, differential cellular ATP levels denoting changes in cell metabolism were observed in both cell types as a result of exposure to the SiNP nanoform (Table 3). Also, since these SiNP nanoforms were custom-synthesized to have a series of sizes with uncoated (pristine) and coated SiNPs, this enabled the assessment of size-, dose-, and modification-related effects on cytotoxicity. Based on the consensus cytotoxic potency (β_{avg}) data (Table 3), SiNP particles with contrasting cytotoxic potencies were selected to contain fewer particles, yet to be able to address the effect of size (15, 30, and 75 nm uncoated), and within one size the effect of modification (within 15 nm of different surface modifications) for further testing for mechanistic information such as oxidative stress and proteomic analysis.

The findings on cytotoxicity of TiNPs in the two cell types revealed dose- and treatment-main effects with assay-specific and cell type-specific differences in responses (Figures S3a−c and S4a−c). The TiNP nanoforms used in this work varied in size, surface coating, as well as crystal structure, which can influence the toxicity findings. Although nanoform-specific cellular cytotoxic responses were observed in both cell types, cell type-specific toxicity responses were observed with cellular ATP levels, where most NPs and J774A.1 cells exhibited greater β_{ATP} values and slopes of dose−response relationships compared to those of A549 cells after exposure of these nanoforms (Table 4 and Figures S3a and S4c). Also, a comparison of relative cytotoxic potencies (average potency estimate β averaged values for both cell types) of uncoated 50 nm TiNP nanoforms with different crystal structures (Ti-03 vs Ti-05) showed that the anatase form Ti-03 was relatively more cytotoxic than the rutile form Ti-05, in both cell types (Table 4). These findings are consistent with previous reports, where the anatase structure of nanoTiNP was reported to be relatively more reactive compared to the rutile form and attributed to the larger surface area.[66] There are also reports relating the crystalline phase and the related increase in the surface area to enhance the ability to generate reactive oxygen species, especially in the case of nanoTiO_2.[71,72] In this work, we observed (Table 2) an increased BET surface area and increased DLS size (agglomeration state in solution) for Ti-03 (anatase form) compared to Ti-05 (rutile form). Ti-11, a nanowire, was found to be more potent than the other nanoforms in both cell types. It was also observed that, in general, exposure to relatively larger-size nanoparticles, whether coated or uncoated, affected J774A.1 cells more than A549 cells.

Cell type-specific differences in potency ranking for both SiNP and TiNP nanoform exposure may imply differences in cell−particle interactions and the resulting particle uptake by these cells. Furthermore, correlation analysis results between the physicochemical characteristics and average cytotoxic potencies identified TEM size, DLS size, surface area (SA), and surface groups (TGA results) appeared to be determinants of cytotoxicity for SiNP nanoforms in A549 lung epithelial cells, while DLS size and surface charge indicated by ζ-potential (ZP) and surface groups were identified as descriptors of cytotoxic potency in J774A.1 monocyte/macrophage cells. DLS values reflecting the agglomeration states of custom-synthesized SiNP nanoforms used in this work were in concordance with the agglomeration behavior of commercially available amorphous silica,[35] where agglomeration state was attributed to the concentration of particles in solution and to the presence of FBS.

For TiNP nanoform exposures, total and transition metal contents appeared to be descriptors of A549 cell cytotoxic potency (significant correlation), with DLS size showing some correlation trends. It has been reported previously that these TiNPs are negligibly soluble,[73] and solubility may contribute less to the toxicity of these TiNPs. Meanwhile, TEM, DLS size, surface area, and transition metal content appeared to be potent determinants of cytotoxicity for these NP-exposed J774A.1 cells. These findings are in line with previous reports on the association between physicochemical characteristics and toxicity of nanoparticles.[35,43]

For mechanistic analysis, we used exposure doses of 30 $\mu g/cm^2$ and below to avoid examination at doses that caused frank toxicity (high doses where cell death is noticeable) based on cytotoxicity information. Although environmentally relevant doses can be relatively low, these are the typical doses employed in *in vitro* exposure studies to gain mechanistic information.

https://doi.org/10.1021/acs.jproteome.4c00651
J. Proteome Res. 2025, 24, 1672−1687

Cellular oxidative stress levels post-SiNP exposure exhibited cell type-related differences. Exposure to all amorphous SiNP nanoforms led to cellular oxidative stress. Also, it was observed that the 15 nm-coated C-11 SiNP nanoform elicited relatively more GSH oxidation in A549 lung epithelial cells (Figure 1A) as opposed to the larger uncoated particles (75 and 100 nm). In J774A.1 cells (Figure 1A), these larger uncoated particles led to increased oxidative stress compared to those of the other nanoforms tested. These cell type-specific observations are in line with the cytotoxic potency β_{avg} values for these nanoforms (Table 3). Furthermore, for SiNP-exposed cells, the cytotoxic potency β_{avg} was negatively correlated with the GSH/GSSG ratio (A549: $r = -0.24$ (not significant); J774A.1: $r = -0.81$ ($p < 0.01$)), suggesting the contribution of oxidative stress to cellular cytotoxicity in both cell types exposed to SiNPs. These findings are consistent with the oxidative potential of amorphous SiNPs.[42,74] There are also studies that report reactive oxygen species ROS formation as one of the mechanisms by which SiNPs can exert toxicity.[75−80]

Meanwhile, exposure to all TiNP nanoforms led to oxidative stress in both A549 lung epithelial and J774A.1 monocyte/macrophage cells, with the latter showing more GSH transformation. The findings on TiNP exposure-related cellular oxidative stress are consistent with previous reports on the ability of nanoTiO_2 to participate in electron transfer reactions[81] and oxidative stress after both *in vitro* and *in vivo* exposure to TiNPs.[82,83] Similar to the cytotoxicity findings, among the TiNP nanoforms with different crystal structures, the anatase form (Ti-03) displayed increased oxidative capacity compared to the rutile form (Ti-05), for both exposed cell types (Figure 1B), which can be attributed to the relatively increased surface area of the Ti-03 nanoform in contrast to Ti-05, as mentioned before, which is consistent with previous reports.[71,72] Also, for TiNP exposure, the cytotoxic potency β_{avg} was negatively correlated with the GSH/GSSG ratio (A549: $r = -0.20$ (not sig); J774A.1: $r = -0.10$ (not sig)), suggesting that TiNP exposure-related cellular oxidative stress can contribute to DNA damage, inflammation, and cell injury, which is reflected through changes in cellular pathways and related biological processes (Figures 2 and 3) as well as observed cytotoxicity responses, in line with previous findings.[66,73]

In this work, we analyzed secreted proteins in cell supernatants using targeted antibody-based multiplexed array analysis, while cellular proteins were analyzed by an untargeted LC-orbitrap mass spectrometry method. Also, due to the exploratory nature of this work, we only focused on a (10−100 kDa) fraction of the cellular proteins to reduce complexity and to ensure that there was no interference due to the presence of nanoparticles on protein profiles. Both secreted and cellular protein information were combined for pathway analysis. Pathway enrichment analysis identified some common pathways that were perturbed as a result of cell exposure to nanoforms of SiNPs and TiNPs. Nevertheless, nanoform-, dose- and cell type-specific responses (up/or downregulation) were observed, as illustrated by the heatmaps with hierarchical clustering information (Figure 2). A549 cells exposed to SiO_2 and TiO_2 nanoforms exhibited perturbations in mechanistic pathways, including Rho GTPase signaling, cellular response to stress, cytokine signaling, metabolism, cell cycle, and protein post-translational modification. Meanwhile, J774A.1 cells exposed to the nanoforms of SiO_2 and TiO_2 also reflected changes in some common pathways, namely, GPCR signaling, MAPK signaling, AP-1 transcription factor network, chemokine, and cytokine signaling pathways. (Figure 2A−D). Although some common pathways were found to be affected by exposure to these nanoparticles, nanoform- as well as dose-specific differences were observed in the pathway profiles (up/down regulation) for nanoSiO_2 and nanoTiO_2 for the two different cell types. Also, for SiNP-exposed A549 cells, the cytotoxic potency β_{avg} was positively correlated with secreted IL-8 ($r = 0.10$ (did not reach significance)), and for J774A.1 cells, the cytotoxic potency β was positively correlated with secreted TNFα ($r = 0.43$ (did not reach significance)), where IL-8 and TNFα are proinflammatory cytokines, suggesting some contribution of the inflammatory process to cellular cytotoxicity for both cell types exposed to SiNPs. Similarly, with TiNP exposure, the cytotoxic potency β_{avg} was positively correlated with secreted TNFα ($r = 0.48$, $p = 0.12$) for J774A.1 cells; for A549 cells exposed to uncoated TiNP nanoforms, positive correlation was observed between β_{avg} and secreted IL-8 ($r = 0.83$, $p = 0.058$), suggesting that inflammatory process also contributes to TiNP exposure-related cellular cytotoxicity responses. Meanwhile, the analysis of associations between NP (for both SiNP and TiNP nanoforms) exposure-related cellular GSH/GSSG ratio and cell-released cytokines showed, in general, a negative correlation for both cell types (e.g., SiNP-exposed A549: $r = -0.67$, $p = 0.058$), suggesting a positive association between NP exposure-related oxidative stress and the inflammatory process, implying that oxidative stress may contribute to the inflammatory process, as reported previously for other metal oxide nanoparticles.[66,84]

Moreover, biological processes affected by SiNP and TiNP exposure based on the A549 cellular pathway findings (leading-edge proteins, Table S1) and GO biological process results (Figure 3) were linked to vesicle-mediated transport (clathrin-mediated endocytosis),[85] oxidative stress, protein post-translational modification, immune/inflammatory processes, DNA damage, oxidative phosphorylation/mitochondria, metabolism, apoptosis/cell death, cell adhesion, and cell cycle. Of these, oxidative and inflammatory processes and their association (correlation analysis data) with cellular cytotoxic potency β support the pathway analysis findings. These mechanistic insights can contribute to the refinement/validation of the adverse outcome pathway (AOP) model, enabling health risk analysis. Additionally, the A549 cells exposed to nanoSiO_2 showed effects related to scavenger receptor-mediated endocytosis (e.g., STAB2) as well as autophagy, as reported previously,[86,87] providing some insights into NP−cell interactions. The proteins involved in the pathways affected by SiNP and TiNP exposure were identified to be different for the two particle types in this work, even though they are related to similar biological processes. Furthermore, it was interesting to note that A549 cells exposed to some SiNP nanoforms at high doses showed downregulated pathways related to selected immune/inflammatory processes, while, high-dose exposure to TiNP led to mostly upregulated pathways compared to that at low doses, with the exception of the TiNP nanoform Ti-11, which is a nanowire that displayed downregulation in specific immune/inflammatory pathways as well as pathways relevant to oxidative stress, at both low and high doses of exposure. Low- and high-dose exposure-related protein changes may be due to differences in solubility properties or the shapes of nanoforms. For instance, in the case of Ti-11, the shape may perhaps influence NP−cell interaction modes and subsequent related protein responses, consistent with relatively higher cellular cytotoxic potency (β_{avg}). Similar patterns of dampening of oxidative stress as well as immune/inflammatory processes have been observed

https://doi.org/10.1021/acs.jproteome.4c00651
J. Proteome Res. 2025, 24, 1672−1687

previously with air particle exposure.[88] Biological process related to J774A.1 cellular pathway impacted by SiNP and TiNP exposure included defense mechanisms (consistent with the functionality of this phagocytic host−defense cell type), oxidative stress, protein post-translational modification, immune/inflammatory processes, metabolism, and apoptosis/cell death (leading-edge proteins, Table S1 and Figure 3). These findings are consistent with previous reports on cellular pathways/biological processes affected by SiNPs and TiNPs, as identified by various *in vitro* and *in vivo* exposure studies.[35,39,40,43,89] Dose- and nanoform-specific influences on these pathways are in line with the observed cell type-specific cytotoxicity and oxidative stress responses.

In our previous work on J774A.1 cells exposed to some nanoforms of SiNPs, we have shown localization of nanoparticles in cytoplasmic vesicles, in the vicinity of organelles, including nucleus, mitochondria, and endoplasmic reticulum by TEM analysis, as well as large vacuoles, autophagosomes, loss of cristae in mitochondria and vacuolated mitochondria,[39] which is consistent with the findings of this study. Both *in vitro* and *in vivo* exposure to SiNP or TiNP and cellular/organ-level toxicity (e.g., respiratory, immune, and reproductive systems) and mitochondrial dysfunction have been reported earlier.[83,90−96] We have also recently exposed zebrafish embryos to members of the SiNPs and TiNPs tested in this work as an alternative *in vivo* toxicity testing platform and observed NP exposure-related oxidative stress response in the embryos by immunofluorescence (DCFH-DA) and observed protein changes (decrease in superoxide dismutase-SOD2 and increase in barrier-to-autointegration factor) related to heightened oxidative stress after NP exposures (preliminary unpublished information). Also, mitochondrial function-related protein changes (decreased ATP synthase and cytochrome c oxidase subunits) were observed in the embryo tissues (data not shown), implying adverse mitochondrial effects after NP exposure, which is in line with decreased cellular ATP levels (β_{ATP}) as well as the observed proteomic changes after *in vitro* NP exposure of the two cell types, in the current study.

The in vitro or *in vivo* toxicity of environmental chemicals, including ENMs, has been traditionally examined using one or few cytotoxicity or systemic or physiological endpoints, for risk characterization related to these exposures. Currently, there is a shift toward the application of high-throughput *in vitro* exposure models in combination with high-content molecular-level analysis (e.g., Omics) as new approach methodologies (NAMs), in an effort to move away from the use of vertebrate animals in toxicity testing. There are relatively more reports on transcriptomic and metabolomic analysis for chemical toxicity testing, and lately, proteomic approaches are being considered for this purpose.[15,97−99] Proteomic screening for chemical toxicity-related molecular-level information can advance the validation and refinement of conceptual models (e.g., adverse outcome pathway (AOP)) used in health risk analysis. Besides, proteomic information, either independently or integrated with other OMIC data (multi-Omic approaches), can enable exposure-specific biomarker development for rapid/cost-effective high-volume sample analysis. Although the proteomic analysis in this work was exploratory and not exhaustive, it provided new insights into key biological events of toxicity (e.g., oxidative stress, inflammatory process, cell cycle, and metabolism/mitochondrial effects) associated with SiNP and TiNP nanoform exposures in multiple cell types, consistent with the observed cytotoxicity responses. The findings from this work on *in vitro* NP exposure-related alterations in inflammatory pathways are in line with recent work on the first human-controlled acute exposure of healthy volunteers to nanoparticles (graphene oxide), suggesting some perturbations in the inflammatory process identified by toxicity testing using plasma proteomics and lipidomics,[100] irrespective of the nanoparticle type used in the latter work. The current *in vitro* study findings on relative cytotoxic potencies, potential underlying mechanisms, and physicochemical determinants of toxicity not only advance health risk analysis of these SiNP and TiNP nanoforms but also can potentially enable the selection of less toxic nanoforms for different applications.

CONCLUSIONS

Nanoforms of both SiO_2 and TiO_2 exhibited dose-, cell type-, and NP-specific cellular cytotoxicity. Size, agglomeration, surface modification, and metal impurities appeared to be some of the important cytotoxicity determinants. Besides, the crystal structure and shape also influenced the cytotoxicity due to TiNP exposure. Cellular pathways affected by SiO_2 and TiO_2 nanoforms identified some endocytosis-related processes for A549 epithelial cells, while host defense-related mechanisms were observed in J774A.1 cells, suggesting cell-specific differences relevant to particle uptake mechanisms. Other biological processes affected by exposure to SiNP and TiNP nanoforms in these cell types included oxidative stress, inflammatory processes, cell cycle-related effects, metabolism, and apoptosis/cell death. In addition, the correlation between cellular oxidative stress, inflammatory pathway, and cytotoxic potency adds value in terms of revealing the molecular basis of the toxicity of these nanoforms, which is valuable information for human health risk analysis. These findings warrant future work on high-content proteomic applications in nanotoxicology to unravel the mechanistic pathways underlying the toxicity of these manufactured nanomaterials.

ASSOCIATED CONTENT

Supporting Information

The Supporting Information is available free of charge at https://pubs.acs.org/doi/10.1021/acs.jproteome.4c00651.

NP exposure-related biological process, attributed to leading-edge proteins identified by pathway enrichment analysis (Table S1); cytotoxicity analysis in A549 cells exposed to different nanoforms of SiNPs, and dose and surface modification, and size-specific cellular cytotoxicity responses of A549 cells exposed to different nanoforms of SiNPs (Figure S1); cytotoxicity analysis in J774A.1 cells exposed to different nanoforms of SiNPs, and dose-, surface modification, and size-specific cellular cytotoxicity responses of J774A.1 cells exposed to different nanoforms of SiNPs (Figure S2); cytotoxicity analysis in A549 cells exposed to different nanoforms of TiNPs, and dose- and treatment-specific cellular cytotoxicity responses of A549 cells exposed to different nanoforms of TiNPs (Figure S3); cytotoxicity analysis in J774A.1 cells exposed to different nanoforms of TiNPs, and dose- and treatment-specific cellular cytotoxicity responses of J774A.1 cells exposed to different nanoforms of TiNPs (Figure S4). (PDF)

https://doi.org/10.1021/acs.jproteome.4c00651
J. Proteome Res. 2025, 24, 1672−1687

AUTHOR INFORMATION

Corresponding Author

Premkumari Kumarathasan − *Environmental Health Science and Research Bureau, HECSB, Health Canada, Ottawa, Ontario, Canada K1A 0K9; Faculty of Health Sciences, University of Ottawa, Ottawa, Ontario, Canada K1N 6N5;* orcid.org/0000-0001-7239-4967; Phone: 613-218-4530; Email: premkumari.kumarathasan@hc-sc.gc.ca

Authors

Nazila Nazemof − *Environmental Health Science and Research Bureau, HECSB, Health Canada, Ottawa, Ontario, Canada K1A 0K9; Faculty of Health Sciences, University of Ottawa, Ottawa, Ontario, Canada K1N 6N5*

Erica Blais − *Environmental Health Science and Research Bureau, HECSB, Health Canada, Ottawa, Ontario, Canada K1A 0K9*

Krishna Priya Syama − *Environmental Health Science and Research Bureau, HECSB, Health Canada, Ottawa, Ontario, Canada K1A 0K9*

Dalibor Breznan − *Environmental Health Science and Research Bureau, HECSB, Health Canada, Ottawa, Ontario, Canada K1A 0K9*

Yasmine Dirieh − *Environmental Health Science and Research Bureau, HECSB, Health Canada, Ottawa, Ontario, Canada K1A 0K9*

Hiroyuki Aoki − *Department of Biochemistry, University of Regina, Regina, Saskatchewan, Canada S4S 0A2*

Sadhna Phanse − *Department of Biochemistry, University of Regina, Regina, Saskatchewan, Canada S4S 0A2*

Azam Tayabali − *Environmental Health Science and Research Bureau, HECSB, Health Canada, Ottawa, Ontario, Canada K1A 0K9*

Mohan Babu − *Department of Biochemistry, University of Regina, Regina, Saskatchewan, Canada S4S 0A2*

Complete contact information is available at: https://pubs.acs.org/10.1021/acs.jproteome.4c00651

Author Contributions

This manuscript was written through the contributions of all authors. All authors have given approval to the final version of the manuscript. P.K. contributed to the design and execution of the study, data analysis, statistical analysis, data interpretation, and writing of the manuscript. N.N. contributed to ENM exposure, cytotoxicity assays, and associated data analysis and writing of the manuscript. E.B. contributed to the proteomic sample processing, data handling, statistical analysis, and the preparation of the manuscript. K.P.S. contributed to data analysis, data preparation, and writing of the manuscript. D.B. contributed to the study design, cell culture exposure experiments, and data analysis. Y.D. supported with multiplex protein array analysis of secreted proteins and data handling. H.A. conducted all LC-MS analyses and contributed to the writing of the manuscript. S.P. carried out all bioinformatic analyses, including protein identification and uploading to PRIDE, pathway analysis, and writing of the manuscript. A.T. contributed to the study design, multiplex protein array analysis, and review. M.B. contributed to mass spectrometry analysis, review, and writing of the manuscript.

Funding

This work was funded by the Chemicals Management Plan (CMP) and the Nanotechnology Section, New Substances Assessment and Control Bureau (NSACB) of Health Canada (CRA). Open access funded by the Health Canada Library

Notes

The authors declare no competing financial interest.

ACKNOWLEDGMENTS

A panel of amorphous SiNPs was synthesized by Applied Quantum Materials Inc. (Edmonton, AB, Canada). We would like to pay tribute to Dr. Renaud Vincent, who had contributed to the inception and conduct of this work and our irreparable recent loss of him while we were finalizing the manuscript is deeply felt by all of us. We are grateful to Drs. Linda Johnston and David Kennedy from NRC Canada for providing TiNP nanoforms and information on DLS, functional group analysis, and surface area for these particles, and Dr. Nimal DeSilva at the Department of Earth and Environmental Sciences, University of Ottawa, for conducting the ICP-MS/AES analysis.

REFERENCES

(1) Rahman, A.; Kumarathasan, P.; Gomes, J. Infant and Mother Related Outcomes from Exposure to Metals with Endocrine Disrupting Properties during Pregnancy. *Sci. Total Environ.* **2016**, *569*−*570*, 1022−1031.

(2) Borghese, M. M.; Huang, R.; MacPherson, S.; Gaudreau, E.; Gagné, S.; Ashley-Martin, J.; Fisher, M.; Booij, L.; Bouchard, M. F.; Arbuckle, T. E. A Descriptive Analysis of First Trimester Urinary Concentrations of 14 Bisphenol Analogues in the MIREC Canadian Pregnancy Cohort. *Int. J. Hyg. Environ. Health* **2023**, *253*, No. 114225.

(3) Ferguson, K. K.; Peterson, K. E.; Lee, J. M.; Mercado-García, A.; Blank-Goldenberg, C.; Téllez-Rojo, M. M.; Meeker, J. D. Prenatal and Peripubertal Phthalates and Bisphenol A in Relation to Sex Hormones and Puberty in Boys. *Reprod. Toxicol.* **2014**, *47*, 70−76.

(4) Rajkumar, A.; Luu, T.; Beal, M. A.; Barton-Maclaren, T. S.; Robaire, B.; Hales, B. F. Elucidation of the Effects of Bisphenol A and Structural Analogs on Germ and Steroidogenic Cells Using Single Cell High-Content Imaging. *Toxicol. Sci.* **2021**, *180* (2), 224−238.

(5) Palaniyandi, J.; Bruin, J. E.; Kumarathasan, P.; MacPherson, S.; Borghese, M. M.; Ashley-Martin, J. Prenatal Exposure to Perfluoroalkyl Substances and Inflammatory Biomarker Concentrations. *Environ. Epidemiol.* **2023**, *7* (4), No. e262.

(6) Vincent, R.; Kumarathasan, P.; Goegan, P.; Bjarnason, S. G.; Guénette, J.; Karthikeyan, S.; Thomson, E. M.; Adamson, I. Y.; Watkinson, W. P.; Battistini, B.; Miller, F. J. Acute Cardiovascular Effects of Inhaled Ambient Particulate Matter: Chemical Composition-Related Oxidative Stress, Endothelin-1, Blood Pressure, and ST-Segment Changes in Wistar Rats. *Chemosphere* **2022**, *296*, No. 133933.

(7) Calderón-Garcidueñas, L.; Ayala, A. Air Pollution, Ultrafine Particles, and Your Brain: Are Combustion Nanoparticle Emissions and Engineered Nanoparticles Causing Preventable Fatal Neurodegenerative Diseases and Common Neuropsychiatric Outcomes? *Environ. Sci. Technol.* **2022**, *56* (11), 6847−6856.

(8) Kumah, E. A.; Fopa, R. D.; Harati, S.; Boadu, P.; Zohoori, F. V.; Pak, T. Human and Environmental Impacts of Nanoparticles: A Scoping Review of the Current Literature. *BMC Public Health* **2023**, *23* (1), 1059.

(9) WHO https://www.who.int/publications-detail-redirect/9789241550048 (accessed February 14, 2024).

(10) Vance, M. E.; Kuiken, T.; Vejerano, E. P.; McGinnis, S. P.; Hochella, M. F.; Rejeski, D.; Hull, M. S. Nanotechnology in the Real World: Redeveloping the Nanomaterial Consumer Products Inventory. *Beilstein J. Nanotechnol.* **2015**, *6*, 1769−1780.

(11) Environment and Climate Change Canada. Data Gap Analysis of Nanoscale Forms of Substances on the Domestic Substances List: A

Human Health Perspective. https://www.canada.ca/en/environment-climate-change/services/canadian-environmental-protection-act-registry/data-gap-analysis-nanoscale-domestic-substances-list.html (accessed February 16, 2024).
(12) Yang, X.; He, C.; Li, J.; Chen, H.; Ma, Q.; Sui, X.; Tian, S.; Ying, M.; Zhang, Q.; Luo, Y.; Zhuang, Z.; Liu, J. Uptake of Silica Nanoparticles: Neurotoxicity and Alzheimer-like Pathology in Human SK-N-SH and Mouse Neuro2a Neuroblastoma Cells. *Toxicol. Lett.* **2014**, *229* (1), 240−249.
(13) Sripanyakorn, S.; Jugdaohsingh, R.; Dissayabutr, W.; Anderson, S. H. C.; Thompson, R. P. H.; Powell, J. J. The Comparative Absorption of Silicon from Different Foods and Food Supplements. *Br. J. Nutr.* **2009**, *102* (6), 825−834.
(14) Lee, J.-H.; Kang, S.; Ahn, M.; Jang, H.; Min, D.-H. Development of Dual-Pore Coexisting Branched Silica Nanoparticles for Efficient Gene-Chemo Cancer Therapy. *Small* **2018**, *14* (7), No. 1702564, DOI: 10.1002/smll.201702564.
(15) Li, K.; Li, J.-L.; Zheng, D.-W.; Zeng, X.; Liu, C.-J.; Zhang, X.-Z. A Modular Theranostic Platform for Tumor Therapy and Its Metabolic Studies. *J. Mater. Chem. B* **2019**, *7* (17), 2790−2798.
(16) Morais, R. P.; Hochheim, S.; de Oliveira, C. C.; Riegel-Vidotti, I. C.; Marino, C. E. B. Skin Interaction, Permeation, and Toxicity of Silica Nanoparticles: Challenges and Recent Therapeutic and Cosmetic Advances. *Int. J. Pharm.* **2022**, *614*, No. 121439.
(17) Thabet, A. F.; Boraei, H. A.; Galal, O. A.; El-Samahy, M. F. M.; Mousa, K. M.; Zhang, Y. Z.; Tuda, M.; Helmy, E. A.; Wen, J.; Nozaki, T. Silica Nanoparticles as Pesticide against Insects of Different Feeding Types and Their Non-Target Attraction of Predators. *Sci. Rep.* **2021**, *11* (1), No. 14484.
(18) Mebert, A. M.; Baglole, C. J.; Desimone, M. F.; Maysinger, D. Nanoengineered Silica: Properties, Applications and Toxicity. *Food Chem. Toxicol.* **2017**, *109* (Pt 1), 753−770.
(19) Wang, T.; Jiang, H.; Wan, L.; Zhao, Q.; Jiang, T.; Wang, B.; Wang, S. Potential Application of Functional Porous TiO2 Nanoparticles in Light-Controlled Drug Release and Targeted Drug Delivery. *Acta Biomater.* **2015**, *13*, 354−363.
(20) Foster, H. A.; Ditta, I. B.; Varghese, S.; Steele, A. Photocatalytic Disinfection Using Titanium Dioxide: Spectrum and Mechanism of Antimicrobial Activity. *Appl. Microbiol. Biotechnol.* **2011**, *90* (6), 1847−1868.
(21) Çeşmeli, S.; Biray Avci, C. Application of Titanium Dioxide (TiO2) Nanoparticles in Cancer Therapies. *J. Drug Target.* **2019**, *27* (7), 762−766.
(22) Weir, A.; Westerhoff, P.; Fabricius, L.; Hristovski, K.; von Goetz, N. Titanium Dioxide Nanoparticles in Food and Personal Care Products. *Environ. Sci. Technol.* **2012**, *46* (4), 2242−2250.
(23) Piccinno, F.; Gottschalk, F.; Seeger, S.; Nowack, B. Industrial Production Quantities and Uses of Ten Engineered Nanomaterials in Europe and the World. *J. Nanopart. Res.* **2012**, *14* (9), 1109.
(24) Ziental, D.; Czarczynska-Goslinska, B.; Mlynarczyk, D. T.; Glowacka-Sobotta, A.; Stanisz, B.; Goslinski, T.; Sobotta, L. Titanium Dioxide Nanoparticles: Prospects and Applications in Medicine. *Nanomaterials* **2020**, *10* (2), 387.
(25) Stone, V.; Johnston, H.; Clift, M. J. D. Air Pollution, Ultrafine and Nanoparticle Toxicology: Cellular and Molecular Interactions. *IEEE Trans. Nanobiosci.* **2007**, *6* (4), 331−340.
(26) Shi, H.; Magaye, R.; Castranova, V.; Zhao, J. Titanium Dioxide Nanoparticles: A Review of Current Toxicological Data. *Part. Fibre Toxicol.* **2013**, *10*, 15.
(27) Andersson, P. O.; Lejon, C.; Ekstrand-Hammarström, B.; Akfur, C.; Ahlinder, L.; Bucht, A.; Osterlund, L. Polymorph- and Size-Dependent Uptake and Toxicity of TiO_2 Nanoparticles in Living Lung Epithelial Cells. *Small* **2011**, *7* (4), 514−523.
(28) Shukla, S. J.; Huang, R.; Austin, C. P.; Xia, M. The Future of Toxicity Testing: A Focus on In Vitro Methods Using a Quantitative High Throughput Screening Platform. *Drug Discovery Today* **2010**, *15* (23−24), 997.
(29) Inesta-Vaquera, F.; Miyashita, L.; Grigg, J.; Henderson, C. J.; Wolf, C. R. Defining the in Vivo Mechanism of Air Pollutant Toxicity Using Murine Stress Response Biomarkers. *Sci. Total Environ.* **2023**, *888*, No. 164211.
(30) Kolimi, P.; Narala, S.; Youssef, A. A. A.; Nyavanandi, D.; Dudhipala, N. A Systemic Review on Development of Mesoporous Nanoparticles as a Vehicle for Transdermal Drug Delivery. *Nanotheranostics* **2023**, *7* (1), 70−89.
(31) Chang, X.; Zhu, Z.; Weng, L.; Tang, X.; Liu, T.; Zhu, M.; Liu, J.; Tang, W.; Zhang, Y.; Chen, X. Selective Manipulation of the Mitochondria Oxidative Stress in Different Cells Using Intelligent Mesoporous Silica Nanoparticles to Activate On-Demand Immunotherapy for Cancer Treatment. *Small* **2024**, *20*, No. 2307310.
(32) Valdiglesias, V.; Costa, C.; Sharma, V.; Kiliç, G.; Pásaro, E.; Teixeira, J. P.; Dhawan, A.; Laffon, B. Comparative Study on Effects of Two Different Types of Titanium Dioxide Nanoparticles on Human Neuronal Cells. *Food Chem. Toxicol.* **2013**, *57*, 352−361.
(33) Chen, J.; Lei, L.; Mo, W.; Dong, H.; Li, J.; Bai, C.; Huang, K.; Truong, L.; Tanguay, R. L.; Dong, Q.; Huang, C. Developmental Titanium Dioxide Nanoparticle Exposure Induces Oxidative Stress and Neurobehavioral Changes in Zebrafish. *Aquat. Toxicol.* **2021**, *240*, No. 105990.
(34) Gonzalez, L.; Thomassen, L. C. J.; Plas, G.; Rabolli, V.; Napierska, D.; Decordier, I.; Roelants, M.; Hoet, P. H.; Kirschhock, C. E. A.; Martens, J. A.; Lison, D.; Kirsch-Volders, M. Exploring the Aneugenic and Clastogenic Potential in the Nanosize Range: A549 Human Lung Carcinoma Cells and Amorphous Monodisperse Silica Nanoparticles as Models. *Nanotoxicology* **2010**, *4*, 382−395.
(35) Breznan, D.; Das, D. D.; O'Brien, J. S.; MacKinnon-Roy, C.; Nimesh, S.; Vuong, N. Q.; Bernatchez, S.; DeSilva, N.; Hill, M.; Kumarathasan, P.; Vincent, R. Differential Cytotoxic and Inflammatory Potency of Amorphous Silicon Dioxide Nanoparticles of Similar Size in Multiple Cell Lines. *Nanotoxicology* **2017**, *11* (2), 223−235.
(36) Kim, W.; Kim, W. K.; Lee, K.; Son, M. J.; Kwak, M.; Chang, W. S.; Min, J.-K.; Song, N. W.; Lee, J.; Bae, K.-H. A Reliable Approach for Assessing Size-Dependent Effects of Silica Nanoparticles on Cellular Internalization Behavior and Cytotoxic Mechanisms. *Int. J. Nanomed.* **2019**, *14*, 7375−7387.
(37) Medina-Reyes, E. I.; Déciga-Alcaraz, A.; Freyre-Fonseca, V.; Delgado-Buenrostro, N. L.; Flores-Flores, J. O.; Gutiérrez-López, G. F.; Sánchez-Pérez, Y.; García-Cuéllar, C. M.; Pedraza-Chaverri, J.; Chirino, Y. I. Titanium Dioxide Nanoparticles Induce an Adaptive Inflammatory Response and Invasion and Proliferation of Lung Epithelial Cells in Chorioallantoic Membrane. *Environ. Res.* **2015**, *136*, 424−434.
(38) Li, Y.; Zhu, Y.; Zhao, B.; Yao, Q.; Xu, H.; Lv, S.; Wang, J.; Sun, Z.; Li, Y.; Guo, C. Amorphous Silica Nanoparticles Caused Lung Injury through the Induction of Epithelial Apoptosis via ROS/Ca2+/DRP1-Mediated Mitochondrial Fission Signaling. *Nanotoxicology* **2022**, *16* (6−8), 713−732.
(39) Kumarathasan, P.; Nazemof, N.; Breznan, D.; Blais, E.; Aoki, H.; Gomes, J.; Vincent, R.; Phanse, S.; Babu, M. In Vitro Toxicity Screening of Amorphous Silica Nanoparticles Using Mitochondrial Fraction Exposure Followed by MS-Based Proteomic Analysis. *Analyst* **2022**, *147* (16), 3692−3708.
(40) Yazdimamaghani, M.; Moos, P. J.; Ghandehari, H. Global Gene Expression Analysis of Macrophage Response Induced by Nonporous and Porous Silica Nanoparticles. *Nanomedicine Nanotechnol. Biol. Med.* **2018**, *14* (2), 533−545.
(41) OECD https://web-archive.oecd.org/temp/2023-11-23/592932-omics.htm (accessed November 21, 2024).
(42) Breznan, D.; Nazemof, N.; Kunc, F.; Hill, M.; Vladisavljevic, D.; Gomes, J.; Johnston, L. J.; Vincent, R.; Kumarathasan, P. Acellular Oxidative Potential Assay for Screening of Amorphous Silica Nanoparticles. *Analyst* **2020**, *145* (14), 4867−4879.
(43) Breznan, D.; Das, D. D.; MacKinnon-Roy, C.; Bernatchez, S.; Sayari, A.; Hill, M.; Vincent, R.; Kumarathasan, P. Physicochemical Properties Can Be Key Determinants of Mesoporous Silica Nanoparticle Potency in Vitro. *ACS Nano* **2018**, *12* (12), 12062−12079.
(44) Kunc, F.; Kodra, O.; Brinkmann, A.; Lopinski, G. P.; Johnston, L. J. A Multi-Method Approach for Quantification of Surface Coatings on

Commercial Zinc Oxide Nanomaterials. *Nanomaterials* **2020**, *10* (4), 678.
(45) Gonzalez, R. J.; Tarloff, J. B. Evaluation of Hepatic Subcellular Fractions for Alamar Blue and MTT Reductase Activity. *Toxicol. In Vitro* **2001**, *15* (3), 257−259.
(46) Vincent, R.; Goegan, P.; Johnson, G.; Brook, J. R.; Kumarathasan, P.; Bouthillier, L.; Burnett, R. T. Regulation of Promoter-CAT Stress Genes in HepG2 Cells by Suspensions of Particles from Ambient Air. *Toxicol. Sci.* **1997**, *39* (1), 18−32.
(47) Kumarathasan, P.; Williams, G.; Bielecki, A.; Blais, E.; Hemmings, D. G.; Smith, G.; von Dadelszen, P.; Fisher, M.; Arbuckle, T. E.; Fraser, W. D.; Vincent, R. Characterization of Maternal Plasma Biomarkers Associated with Delivery of Small and Large for Gestational Age Infants in the MIREC Study Cohort. *PLoS One* **2018**, *13* (11), No. e0204863.
(48) Tyanova, S.; Temu, T.; Cox, J. The MaxQuant Computational Platform for Mass Spectrometry-Based Shotgun Proteomics. *Nat. Protoc.* **2016**, *11* (12), 2301−2319.
(49) The UniProt Consortium. UniProt: The Universal Protein Knowledgebase. *Nucleic Acids Res.* **2017**, *45* (D1), D158−D169.
(50) Park, C. Y.; Klammer, A. A.; Käll, L.; MacCoss, M. J.; Noble, W. S. Rapid and Accurate Peptide Identification from Tandem Mass Spectra. *J. Proteome Res.* **2008**, *7* (7), 3022−3027.
(51) Kim, S.; Pevzner, P. A. MS-GF+ Makes Progress towards a Universal Database Search Tool for Proteomics. *Nat. Commun.* **2014**, *5*, No. 5277.
(52) The, M.; MacCoss, M. J.; Noble, W. S.; Käll, L. Fast and Accurate Protein False Discovery Rates on Large-Scale Proteomics Data Sets with Percolator 3.0. *J. Am. Soc. Mass Spectrom.* **2016**, *27* (11), 1719−1727.
(53) Subramanian, A.; Tamayo, P.; Mootha, V. K.; Mukherjee, S.; Ebert, B. L.; Gillette, M. A.; Paulovich, A.; Pomeroy, S. L.; Golub, T. R.; Lander, E. S.; Mesirov, J. P. Gene Set Enrichment Analysis: A Knowledge-Based Approach for Interpreting Genome-Wide Expression Profiles. *Proc. Natl. Acad. Sci. U.S.A.* **2005**, *102* (43), 15545−15550.
(54) de Hoon, M. J. L.; Imoto, S.; Nolan, J.; Miyano, S. Open Source Clustering Software. *Bioinformatics* **2004**, *20* (9), 1453−1454.
(55) Saldanha, A. J. Java Treeview–Extensible Visualization of Microarray Data. *Bioinformatics* **2004**, *20* (17), 3246−3248.
(56) Bushell, M.; Beauchemin, S.; Kunc, F.; Gardner, D.; Ovens, J.; Toll, F.; Kennedy, D.; Nguyen, K.; Vladisavljevic, D.; Rasmussen, P. E.; Johnston, L. J. Characterization of Commercial Metal Oxide Nanomaterials: Crystalline Phase, Particle Size and Specific Surface Area. *Nanomaterials* **2020**, *10* (9), 1812.
(57) Uribe-Robles, M.; Ortiz-Islas, E.; Rodriguez-Perez, E.; Valverde, F. F.; Lim, T.; Martinez-Morales, A. A. Targeted Delivery of Temozolomide by Nanocarriers Based on Folic Acid-Hollow TiO2 -Nanospheres for the Treatment of Glioblastoma. *Biomater. Adv.* **2023**, *151*, No. 213442.
(58) Wiklund, L.; Sharma, A.; Muresanu, D. F.; Zhang, Z.; Li, C.; Tian, Z. R.; Buzoianu, A. D.; Lafuente, J. V.; Nozari, A.; Feng, L.; Sharma, H. S. TiO2-Nanowired Delivery of Chinese Extract of Ginkgo Biloba EGb-761 and Bilobalide BN-52021 Enhanced Neuroprotective Effects of Cerebrolysin Following Spinal Cord Injury at Cold Environment. *Adv. Neurobiol.* **2023**, *32*, 353−384.
(59) Fruijtier-Pölloth, C. The Toxicological Mode of Action and the Safety of Synthetic Amorphous Silica-a Nanostructured Material. *Toxicology* **2012**, *294* (2−3), 61−79.
(60) Rabolli, V.; Thomassen, L. C. J.; Princen, C.; Napierska, D.; Gonzalez, L.; Kirsch-Volders, M.; Hoet, P. H.; Huaux, F.; Kirschhock, C. E. A.; Martens, J. A.; Lison, D. Influence of Size, Surface Area and Microporosity on the in Vitro Cytotoxic Activity of Amorphous Silica Nanoparticles in Different Cell Types. *Nanotoxicology* **2010**, *4* (3), 307−318.
(61) Rabolli, V.; Lo Re, S.; Uwambayinema, F.; Yakoub, Y.; Lison, D.; Huaux, F. Lung Fibrosis Induced by Crystalline Silica Particles Is Uncoupled from Lung Inflammation in NMRI Mice. *Toxicol. Lett.* **2011**, *203* (2), 127−134.
(62) L Browning, C.; The, T.; Mason, M. D.; Wise, J. P. Titanium Dioxide Nanoparticles Are Not Cytotoxic or Clastogenic in Human Skin Cells. *J. Environ. Anal. Toxicol.* **2014**, *04* (6), 239.
(63) Brassolatti, P.; de Almeida Rodolpho, J. M.; Franco de Godoy, K.; de Castro, C. A.; Flores Luna, G. L.; Dias de Lima Fragelli, B.; Pedrino, M.; Assis, M.; Nani Leite, M.; Cancino-Bernardi, J.; Speglich, C.; Frade, M. A.; de Freitas Anibal, F. Functionalized Titanium Nanoparticles Induce Oxidative Stress and Cell Death in Human Skin Cells. *Int. J. Nanomed.* **2022**, *17*, 1495−1509.
(64) Chen, Z.; Wang, Y.; Ba, T.; Li, Y.; Pu, J.; Chen, T.; Song, Y.; Gu, Y.; Qian, Q.; Yang, J.; Jia, G. Genotoxic Evaluation of Titanium Dioxide Nanoparticles in Vivo and in Vitro. *Toxicol. Lett.* **2014**, *226* (3), 314−319.
(65) Zlomanov, V. P.; Khoviv, A. M.; Zavrazhnov, A. J.; Zlomanov, V. P.; Khoviv, A. M.; Zavrazhnov, A. J. Physicochemical Analysis and Synthesis of Nonstoichiometric Solids. In *Materials Science − Advanced Topics*; IntechOpen, 2013.
(66) Shabbir, S.; Kulyar, M. F.-E.-A.; Bhutta, Z. A.; Boruah, P.; Asif, M. Toxicological Consequences of Titanium Dioxide Nanoparticles (TiO2NPs) and Their Jeopardy to Human Population. *BioNanoScience* **2021**, *11* (2), 621−632.
(67) Rasmussen, K.; Rauscher, H.; Mech, A.; Riego Sintes, J.; Gilliland, D.; González, M.; Kearns, P.; Moss, K.; Visser, M.; Groenewold, M.; Bleeker, E. A. J. Physico-Chemical Properties of Manufactured Nanomaterials - Characterisation and Relevant Methods. An Outlook Based on the OECD Testing Programme. *Regul. Toxicol. Pharmacol.* **2018**, *92*, 8−28.
(68) Miyata, R.; van Eeden, S. F. The Innate and Adaptive Immune Response Induced by Alveolar Macrophages Exposed to Ambient Particulate Matter. *Toxicol. Appl. Pharmacol.* **2011**, *257* (2), 209−226.
(69) Boyadzhiev, A.; Solorio-Rodriguez, S. A.; Wu, D.; Avramescu, M.-L.; Rasmussen, P.; Halappanavar, S. The High-Throughput In Vitro CometChip Assay for the Analysis of Metal Oxide Nanomaterial Induced DNA Damage. *Nanomaterials* **2022**, *12* (11), 1844.
(70) European Commission. Solubility of Synthetic Amorphous Silica (SAS). https://health.ec.europa.eu/publications/solubility-synthetic-amorphous-silica-sas_en (accessed November 21, 2024).
(71) Jiang, J.; Oberdörster, G.; Elder, A.; Gelein, R.; Mercer, P.; Biswas, P. Does Nanoparticle Activity Depend upon Size and Crystal Phase? *Nanotoxicology* **2008**, *2* (1), 33−42.
(72) Jin, C.; Tang, Y.; Yang, F. G.; Li, X. L.; Xu, S.; Fan, X. Y.; Huang, Y. Y.; Yang, Y. J. Cellular Toxicity of TiO2 Nanoparticles in Anatase and Rutile Crystal Phase. *Biol. Trace Elem. Res.* **2011**, *141* (1−3), 3−15.
(73) Solorio-Rodriguez, S. A.; Wu, D.; Boyadzhiev, A.; Christ, C.; Williams, A.; Halappanavar, S. A Systematic Genotoxicity Assessment of a Suite of Metal Oxide Nanoparticles Reveals Their DNA Damaging and Clastogenic Potential. *Nanomaterials* **2024**, *14* (9), 743.
(74) Wang, M.; Li, J.; Dong, S.; Cai, X.; Simaiti, A.; Yang, X.; Zhu, X.; Luo, J.; Jiang, L.-H.; Du, B.; Yu, P.; Yang, W. Silica Nanoparticles Induce Lung Inflammation in Mice via ROS/PARP/TRPM2 Signaling-Mediated Lysosome Impairment and Autophagy Dysfunction. *Part. Fibre Toxicol.* **2020**, *17* (1), 23.
(75) Wang, S.; Zhang, J.; Zeng, X.; Zeng, Y.; Wang, S.; Chen, S. Association of Traffic-Related Air Pollution with Children's Neurobehavioral Functions in Quanzhou, China. *Environ. Health Perspect.* **2009**, *117* (10), 1612−1618.
(76) Park, E.-J.; Park, K. Oxidative Stress and Pro-Inflammatory Responses Induced by Silica Nanoparticles in Vivo and in Vitro. *Toxicol. Lett.* **2009**, *184* (1), 18−25.
(77) Ye, Y.; Liu, J.; Xu, J.; Sun, L.; Chen, M.; Lan, M. Nano-SiO2 Induces Apoptosis via Activation of P53 and Bax Mediated by Oxidative Stress in Human Hepatic Cell Line. *Toxicol. In Vitro* **2010**, *24* (3), 751−758.
(78) Guo, C.; Xia, Y.; Niu, P.; Jiang, L.; Duan, J.; Yu, Y.; Zhou, X.; Li, Y.; Sun, Z. Silica Nanoparticles Induce Oxidative Stress, Inflammation, and Endothelial Dysfunction in Vitro via Activation of the MAPK/Nrf2 Pathway and Nuclear Factor-κB Signaling. *Int. J. Nanomed.* **2015**, *10*, 1463−1477.

https://doi.org/10.1021/acs.jproteome.4c00651
J. Proteome Res. 2025, 24, 1672−1687

(79) Chou, C.-C.; Chen, W.; Hung, Y.; Mou, C.-Y. Molecular Elucidation of Biological Response to Mesoporous Silica Nanoparticles in Vitro and in Vivo. *ACS Appl. Mater. Interfaces* **2017**, *9* (27), 22235−22251.
(80) Kusaczuk, M.; Krętowski, R.; Naumowicz, M.; Stypułkowska, A.; Cechowska-Pasko, M. Silica Nanoparticle-Induced Oxidative Stress and Mitochondrial Damage Is Followed by Activation of Intrinsic Apoptosis Pathway in Glioblastoma Cells. *Int. J. Nanomed.* **2018**, *13*, 2279−2294.
(81) Wu, Z.; Li, L.; Zhou, X.; Zhao, X.; Liu, B. Kinetics and Energetic Analysis of the Slow Dispersive Electron Transfer from Nano-TiO2 to O2 by in Situ Diffusion Reflectance and Laplace Transform. *Phys. Chem. Chem. Phys* **2021**, *23* (35), 19901−19910.
(82) Winckers, L. A.; Evelo, C. T.; Willighagen, E. L.; Kutmon, M. Investigating the Molecular Processes behind the Cell-Specific Toxicity Response to Titanium Dioxide Nanobelts. *Int. J. Mol. Sci.* **2021**, *22* (17), 9432.
(83) Li, C.; Tang, M. The Toxicological Effects of Nano Titanium Dioxide on Target Organs and Mechanisms of Toxicity. *J. Appl. Toxicol.* **2024**, *44* (2), 152−164.
(84) Xia, T.; Kovochich, M.; Liong, M.; Mädler, L.; Gilbert, B.; Shi, H.; Yeh, J. I.; Zink, J. I.; Nel, A. E. Comparison of the Mechanism of Toxicity of Zinc Oxide and Cerium Oxide Nanoparticles Based on Dissolution and Oxidative Stress Properties. *ACS Nano* **2008**, *2* (10), 2121−2134.
(85) Qualmann, B.; Mellor, H. Regulation of Endocytic Traffic by Rho GTPases. *Biochem. J.* **2003**, *371* (Pt 2), 233−241.
(86) Campbell, F.; Bos, F. L.; Sieber, S.; Arias-Alpizar, G.; Koch, B. E.; Huwyler, J.; Kros, A.; Bussmann, J. Directing Nanoparticle Biodistribution through Evasion and Exploitation of Stab2-Dependent Nanoparticle Uptake. *ACS Nano* **2018**, *12* (3), 2138−2150.
(87) Zhao, X.; Wu, Y.; Li, J.; Li, D.; Jin, Y.; Zhu, P.; Liu, Y.; Zhuang, Y.; Yu, S.; Cao, W.; Wei, H.; Wang, X.; Han, Y.; Chen, G. JNK Activation-Mediated Nuclear SIRT1 Protein Suppression Contributes to Silica Nanoparticle-Induced Pulmonary Damage via P53 Acetylation and Cytoplasmic Localisation. *Toxicology* **2019**, *423*, 42−53.
(88) Hansson, A.; Rankin, G.; Uski, O.; Friberg, M.; Pourazar, J.; Lindgren, R.; García-López, N.; Boman, C.; Sandström, T.; Behndig, A.; Muala, A. Reduced Bronchoalveolar Macrophage Phagocytosis and Cytotoxic Effects after Controlled Short-Term Exposure to Wood Smoke in Healthy Humans. *Part. Fibre Toxicol.* **2023**, *20* (1), 30.
(89) Chang, H.; Kim, J.; Rho, W.-Y.; Pham, X.-H.; Lee, J. H.; Lee, S. H.; Jeong, D. H.; Jun, B.-H. Silica Nanoparticles. *Adv. Exp. Med. Biol.* **2021**, *1309*, 41−65.
(90) Guo, C.; Wang, J.; Yang, M.; Li, Y.; Cui, S.; Zhou, X.; Li, Y.; Sun, Z. Amorphous Silica Nanoparticles Induce Malignant Transformation and Tumorigenesis of Human Lung Epithelial Cells via P53 Signaling. *Nanotoxicology* **2017**, *11* (9−10), 1176−1194.
(91) Guo, C.; Wang, J.; Jing, L.; Ma, R.; Liu, X.; Gao, L.; Cao, L.; Duan, J.; Zhou, X.; Li, Y.; Sun, Z. Mitochondrial Dysfunction, Perturbations of Mitochondrial Dynamics and Biogenesis Involved in Endothelial Injury Induced by Silica Nanoparticles. *Environ. Pollut.* **2018**, *236*, 926−936.
(92) Napierska, D.; Thomassen, L. C. J.; Lison, D.; Martens, J. A.; Hoet, P. H. The Nanosilica Hazard: Another Variable Entity. *Part. Fibre Toxicol.* **2010**, *7* (1), 39.
(93) Murugadoss, S.; Lison, D.; Godderis, L.; Van Den Brule, S.; Mast, J.; Brassinne, F.; Sebaihi, N.; Hoet, P. H. Toxicology of Silica Nanoparticles: An Update. *Arch. Toxicol.* **2017**, *91* (9), 2967−3010.
(94) Kim, J.-Y.; Park, J.-H.; Kim, M.; Jeong, H.; Hong, J.; Chuck, R. S.; Park, C. Y. Safety of Nonporous Silica Nanoparticles in Human Corneal Endothelial Cells. *Sci. Rep.* **2017**, *7* (1), No. 14566.
(95) Du, Z.; Chen, S.; Cui, G.; Yang, Y.; Zhang, E.; Wang, Q.; Lavin, M. F.; Yeo, A. J.; Bo, C.; Zhang, Y.; Li, C.; Liu, X.; Yang, X.; Peng, C.; Shao, H. Silica Nanoparticles Induce Cardiomyocyte Apoptosis via the Mitochondrial Pathway in Rats Following Intratracheal Instillation. *Int. J. Mol. Med.* **2018**, *43* (3), 1229−1240.
(96) Aschner, M.; Skalny, A. V.; Santamaria, A.; Buha Djordjevic, A.; Tizabi, Y.; Jiang, Y.; Lu, R.; Virgolini, M. B.; Tinkov, A. A. From Mechanisms to Implications: Understanding the Molecular Neurotoxicity of Titanium Dioxide Nanoparticles. *Front. Biosci.* **2023**, *28* (9), 204.
(97) Zhao, X.; Abulikemu, A.; Lv, S.; Qi, Y.; Duan, J.; Zhang, J.; Chen, R.; Guo, C.; Li, Y.; Sun, Z. Oxidative Stress- and Mitochondrial Dysfunction-Mediated Cytotoxicity by Silica Nanoparticle in Lung Epithelial Cells from Metabolomic Perspective. *Chemosphere* **2021**, *275*, No. 129969.
(98) Tollefsen, K. E.; Scholz, S.; Cronin, M. T.; Edwards, S. W.; de Knecht, J.; Crofton, K.; Garcia-Reyero, N.; Hartung, T.; Worth, A.; Patlewicz, G. Applying Adverse Outcome Pathways (AOPs) to Support Integrated Approaches to Testing and Assessment (IATA). *Regul. Toxicol. Pharmacol.* **2014**, *70* (3), 629−640.
(99) Barton-Maclaren, T. S.; Wade, M.; Basu, N.; Bayen, S.; Grundy, J.; Marlatt, V.; Moore, R.; Parent, L.; Parrott, J.; Grigorova, P.; Pinsonnault-Cooper, J.; Langlois, V. S. Innovation in Regulatory Approaches for Endocrine Disrupting Chemicals: The Journey to Risk Assessment Modernization in Canada. *Environ. Res.* **2022**, *204* (Pt C), No. 112225.
(100) Andrews, J. P. M.; Joshi, S. S.; Tzolos, E.; Syed, M. B.; Cuthbert, H.; Crica, L. E.; Lozano, N.; Okwelogu, E.; Raftis, J. B.; Bruce, L.; Poland, C. A.; Duffin, R.; Fokkens, P. H. B.; Boere, A. J. F.; Leseman, D. L. A. C.; Megson, I. L.; Whitfield, P. D.; Ziegler, K.; Tammireddy, S.; Hadjidemetriou, M.; Bussy, C.; Cassee, F. R.; Newby, D. E.; Kostarelos, K.; Miller, M. R. First-in-Human Controlled Inhalation of Thin Graphene Oxide Nanosheets to Study Acute Cardiorespiratory Responses. *Nat. Nanotechnol.* **2024**, *19* (5), 705−714.

https://doi.org/10.1021/acs.jproteome.4c00651
J. Proteome Res. 2025, 24, 1672−1687